82nd International Scientific Conference of the University of Latvia 2024

GEODYNAMICS AND GEOSPATIAL RESEARCH

CONFERENCE PAPERS

Riga, May 30th, 2024

UNIVERSITY OF LATVIA

University of Latvia 82nd International Scientific Conference. Geodynamics and Geospatial Research. Conference Papers. Riga, University of Latvia, 2024, May 30. 49 p.

UNIVERSITY OF LATVIA

#STAND WITH UKRAINE

The conference "Geodynamics and Geospatial Research" organized by the Institute of Geodesy and Geoinformatics of the University of Latvia addresses a wide range of scientific studies and is focused on the interdisciplinarity, versatility and possibilities of research in this wider context in the future to reach more significant discoveries, including business applications and innovations in solutions for commercial enterprises. The research presented at the conference is at different stages of its development and presents the achievements and the intended future. The publication is intended for researchers, students and research social partners as a source of current information and an invitation to join and support these studies.

Prepared under LU Press
Layout designer: Andra Liepiņa

ISBN 978-9934-36-234-7 (PDF)
https://doi.org/10.22364/iscul.82.ggr

PREFACE

The Institute of Geodesy and Geoinformatics of the University of Latvia (LU GGI) in 2024 celebrates its 100th anniversary since the establishment in 1924 and its 30th anniversary since the reestablishment of the Institute of Geodesy in 1994.

The researchers of the Institute of Geodesy (1924–1944) concentrated on the research and education in many advanced topics of that time – development and adjustment of National Geodetic networks, photogrammetry, studies of vertical Earth movement and research in gravimetric and magnetic measurements. Currently the research areas are developed in satellite geodesy and geoinformatics. In this context the main topic of LU GGI activities is concentrated on development of satellite laser ranging systems (SLR), both the hardware and control software, two SLR prototypes were developed until 2010 and the new approach – optical space object observation system is developed and observations have started been started.

The light weight and portable digital zenith camera for studies of vertical deflection has been developed at LU GGI. The test results reach precision of 0.1 arc second which is very promising for the improvement of the quality of the National model of Latvia gravity field modelling. The recent version of the National gravity field developed at the LU GGI has achieved precision of about 2 cm which is much higher than previous model (7–8 cm) used in Latvia. The high precision gravity field model is very important for practice. This reaches correspondingly high precision of normal height determination using Global Navigation Satellite systems (GNSS) in geodetic measurements. This support studies of vertical and horizontal motion of the Earth in Latvia by carrying out the analysis of the GNSS observations at the LatPos and EUPOS-RIGA permanent station networks and LU GGI GNSS stations. These studies provide high quality data for GIS data base development and for digital terrain models of Latvia in general and particular cities of Latvia.

The Institute of Geodesy and Geoinformation is substantial research and development unit of the University of Latvia. The Institutes research activities are organized in two departments – Department of Geodesy and Department of Geoinformation. Within the Department of Geodesy, the major topics of the activities are concentrated on construction of Satellite laser ranging and optical tracking systems (hardware, software), GNSS applications and substantial for developments is participation in the project EUPOS®. Department of Geoinformation is developing 2D and 3D country-wide geographical databases, large urban geographical databases and DEM, and developing highly detailed local geographical databases. Besides the Department of Geodesy has experienced staff dealing with satellite on ground observations.

The LU GGI research is well-known in the professional field in the world, but in Latvia it is an institution that unites and involves leading researchers from all over the country, regardless of their primal work and has become a sort of informal coordinating centre for research in this field. The high scientific quality and applied nature of many studies, presented at this conference, should be highlighted, which will allow to use in the economy this knowledge and numerous scientific solutions already in the next few years.

Director of the Institute of Geodesy and Geoinformatics
Dr. sc. ing. Ingus Mitrofanovs
May 30, 2023

TABLE OF CONTENTS

ON POSITIONAL ASTROMETRIC OBSERVATIONS OF VARIOUS SPACE OBJECTS IN GGI

Diana Haritonova, Ansis Zarins, Augusts Rubans

University of Latvia, Institute of Geodesy and Geoinformatics, Jelgavas str. 3, Riga, Latvia
E-mail: diana.haritonova@lu.lv

Optical tracking system (OTS) of the Institute of Geodesy and Geoinformatics (GGI) has recently proven its ability to perform positional astrometric observations of natural and artificial space objects during the research project "Reconfigurable space object optical tracking system of GGI – implementation stage" and later, using new more advanced CCD matrix. This is a 16.8 Mpix CCD matrix, which ensures a field of view of 0.5° × 0.5°, with pixel size 0.46 arc seconds.

The new camera has ensured detection of stars with the minimum brightness of about 16^m at 1-s exposures, and 18.5^m at 60-s exposures.

For observation purposes, the method of frame stacking in celestial coordinates was used, which allows to prolong the "effective exposure time" of the object, i.e. to increase its brightness. The method has shown that applying it in star tracking mode using 5 frames at different exposures till 60 s, the detectible star magnitude can be increased by 0.7 m – 2.0 m. The results have shown that single frames of shorter exposures (till 5–10 s) are more appropriate for stacking purposes.

Applying the method of frame stacking, it is possible to capture positions of many geostationary satellites and precisely define their coordinates for the given epoch. Additionally, it is possible to increase the brightness of near-Earth objects such as asteroids during one observation session, and representatively show the trajectory of their movement for longer observation period.

In 2021, the SSA Programme (Space Situational Awareness) was promoted to become one of the flagship programmes of the European Union. The programme focuses on three main areas: Near-Earth Objects (NEO), detecting natural objects that can potentially impact Earth; Space Surveillance and Tracking (SST), watching for active and inactive satellites, discarded launch stages and fragmentation debris, and Space Weather (SWE).

The target application area for the optical tracking system of GGI is ground (in-situ) support of space missions, requiring accurate astrometric position determination of satellites, space debris (SST segment), and small Solar system objects (NEO segment).

Acknowledgements

The preparation of the optical tracking system and the research were carried out as a post-doctoral project "Reconfigurable space object optical tracking system of GGI – implementation stage", supported by the European Regional Development Fund activity "Post-doctoral Research Aid", No. 1.1.1.2/VIAA/4/20/619.

Valuable support was given by MikroTik and the University of Latvia Foundation in procurement of new CCD matrix and focuser. Project No. 2283.

RECENT ADVANCES AT THE RIGA SLR STATION

K. Salmins, J. del Pino, J. Kaulins, S. Melkov

University of Latvia, Institute of Astronomy, Jelgavas str. 3, Riga, Latvia
E-mail: kalvis.salmins@lu.lv

This paper reports on some recent advances in the SLR station Riga. We have increased the number of tracked passes covering all the International Laser Ranging Service (ILRS) satellites categories according to the priority lists and are working to maximize the amount of data for the geodetic and high satellites. We have implemented the internal quality control procedures to maintain long- and short-term stability to ensure the ILRS guidelines. Recently, we have successfully determined rotational parameters for several space debris. For the first time we have successfully performed a space debris laser ranging in the multistatic mode when the target is illuminated by the high energy laser and other stations are detecting scattered photons. Part of the activities reported here has been done in the frame of the ESA projects 4000131217/20/NL/SC and 4000135730/21/NL/SC.

ANALYSE OF THE SPECTRAL INDICES OF VERTICAL COORDINATES OF LATVIA'S GNSS PERMANENT STATIONS

Paweł Postek[1], Wiesław Kosek[1], Kamil Maciuk[2]

[1] *Faculty of Production Engineering, University of Life Sciences in Lublin*
[2] *Department of Integrated Geodesy and Cartography, AGH University of Krakow*
E-mail: pawel.postek@up.lublin.pl

The spectral index allows us to understand the dominant frequencies present in time series. It provides valuable insights into the underlying patterns, periodicities, or trends present in the time series, such us information about the balance between low and high frequencies in a time series. In many cases, when the amplitudes of low frequencies become higher than the amplitudes of high frequencies, the spectral index tends to increase.

It is a useful tool in fields such as data science, signal engineering, meteorology, economics, or surveying [1]. Spectral indices of GNSS (Global Navigation Satellite System) coordinate time series allows to analyse their spectral characteristics [2]The Author(s. Similar research were dealing with the analysis of the stability of different measurement techniques [3], seasonal effects [4] or noises in coordinate time series [5].

In this paper author analyse spectral indices of the height component of GNSS times series of 36 Latvian permanent stations. Among them 3: VAIN (Vainode), IRBE (Irbene) and RIGA (Riga) are the permanent stations of the EPN (EUREF Permant Network): As a source of data were used daily PPP (Precise Point Positioning) solutions provided by NGL (Nevada Geodetic Laboratory). Such times series are widely used in a various type of analyses, e.g. determination noise characteristics, seasonal effects or crustal deformations. Fig. 1 shows the map of the spatial distribution of the spectral indices computed by fitting a straight line through robust and linear regression (reglin) to the logarithm of the spectrum as a function of the logarithm of the frequency.

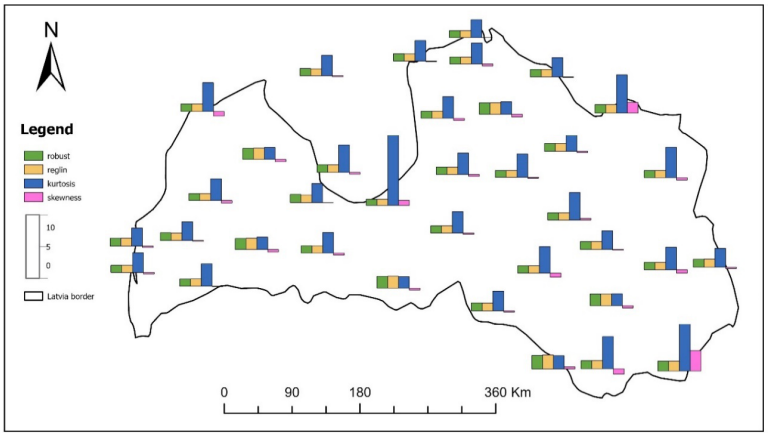

Fig. 1. Values of spectral indices, kurtosis and skewness for the height components of Latvia's permanent GNSS stations

In the analyzed dataset, the robust and reglin indices, which assess noise in time series, show minor differences between the rough estimation method (robust) and linear regression (reglin), indicating stability of measurements under various conditions. To examine whether the analyzed time series meet the conditions for a normal distribution, skewness and kurtosis were calculated. Skewness within the range of – 2 to 2 and kurtosis within the range of 2 to 7 indicate that the time series satisfy the conditions for a normal distribution. Kurtosis is a statistical measure that describes the shape of the probability distribution of a dataset. High Kurtosis greater than 3 indicates more peaked distribution compared to a normal distribution. Low Kurtosis less than 3 indicates lighter tails and a flatter distribution compared to a normal distribution. Kurtosis and skewness values vary significantly between stations. For instance, high kurtosis at the DAGD station suggests that most data are concentrated around the mean, while high skewness indicates the presence of outliers. Such indicators can be useful for identifying anomalies or specific environmental conditions affecting measurements.

References

[1] Montero, D.; Aybar, C.; Mahecha, M.D.; et al. A standardized catalogue of spectral indices to advance the use of remote sensing in Earth system research. *Sci Data 2023 101*. **2023**, 10, 1–20.

[2] Bogusz, J.; Rosat, S.; Klos, A.; et al. On the noise characteristics of time series recorded with nearby located GPS receivers and superconducting gravity meters. *Acta Geod Geophys.* **2018**, 53, 201–220.

[3] Feissel-Vernier, M.; de Viron, O.; Le Bail, K. Stability of VLBI, SLR, DORIS, and GPS positioning. *Earth, Planets Sp.* **2007**, 59, 475–497.

[4] Maciuk, K. The study of seasonal changes of permanent stations coordinates based on weekly EPN solutions. *Artif Satell.* **2016**, 51, 1–18.

[5] Mao, A.; Harrison, C. G. A.; Dixon, T. H. Noise in GPS coordinate time series. *J Geophys Res Solid Earth.* **1999**; 104: 2797–2816.

ESTONIAN NEW GENERATION RTK NETWORKS AND HEIGHT ACCURACY

Harli Jürgenson

Estonian University of Life Sciences. Kreutzwaldi 5, Tartu
E-mail: harli@emu.ee

In Estonia, the use of network RTK have been in progress already more as 15 years. First of all, Trimble opened the Real Time Network (RTN) called as VRSNOW in 2007, then few years later, Topcon did the same. Both networks has about 20 stations. Initially, only GPS+GLONASS corrections were transferred to CMR+ or RTCM31 mount point. Majority of the users paid annual fee and got corrections for everyday survey. As a result of this, the tradition to use of the own base station ended completely. Later on, in 2015, Trimble have added GALILEO and BEIDOU2 to the correction stream. In 2022, BEIDOU3 (third generation BEIDOU) was included as well. The last enhancement increased survey efficiency on forest so much, that 90 % cadastral jobs are made by GNSS devices only. In 2023, third network called MYNET covered whole Estonia as well and shares RTCM32 corrections for all satellites systems using MSM4 messages. Their reference stations are based to CHCNAV devices P5. Same time State Land Board has permanent GNSS reference stations based to Leica receivers. This network is under total renewal process during the current year. But same stations are used for RTK corrections as well, available for state institutions only. The fifth RTN called THEK is founded due to ROAD contraction jobs but covers whole country as well. However, different providers have some different technical details which will be analysed on this paper. For example Trimble VRSNOW correction stream RTCM32 includes MSM4 messages. If we look more deeply inside the stream we can see if there are all signals included or not. Most simple way to do that is to use software called Ntrip Checker. We see all signals except Beidou B3 for on Beidou2 satellites. At the same time B3 is available for Beidou 3 satellites. Similar small problems are visible on every network. MYNET misses Galileo E5ALTBOC which is caused by hardware capabilities. This results Galileo is not used by Trimble devices due to fact that Trimble needs Galileo E5Altboc. Mynet misses Galileo satellites which has number bigger than 30, problem which still needs to be solved.

All RTN in Estonia offer virtual reference point strategy except Thek. In addition to Trimble, Topcon already 10 years offers VRS solution. Later on State land Board based to Leica software does the same. Mynet offer both VRS and connection to closest physical base station. Thek connects users to closest physical base station only. Last choice is selected due to demand for a stable RTK base station for road construction machines (machine control systems).

However, the use of big number of the satellites (like 32) presses down random errors and even the height accuracy is much better as before. Close to any reference station we experience standard deviation 5 mm on 10 minutes series. But even the virtual reference station is created, in case of long distance to closest base stations, we can experience standard deviation 5–20 mm (Fig.). In most cases there are waves on 10 minutes RTK series when point is stored after 1 second for example. But even if the difference of the minimum and maximum value is 6 cm, the mean value of the 10 minutes is very close to real result, in accuracy 1–2 cm.

Due to much more higher efficiency of the RTK receivers not older that 4 years, RTK survey is used much more widely as before, even on constructional geodesy. But still, we have to take account that older receivers are not able to use new generation Beidou satellites, even widely sold Trimble R8s for example. So we need 3 components simultaneously, upgraded RTN, correct corrections stream and modern GNSS RTK device. For many users have been not clear that RTCM32 is needed for triple frequency solutions. For example GPS L5 is not useable by RTCM3.1 correction stream. Several receivers need firmware to be upgraded to be able for RTCM3.2. Taking account those upgrades, we can achieve excellent results on GNSS RTK survey on different applications.

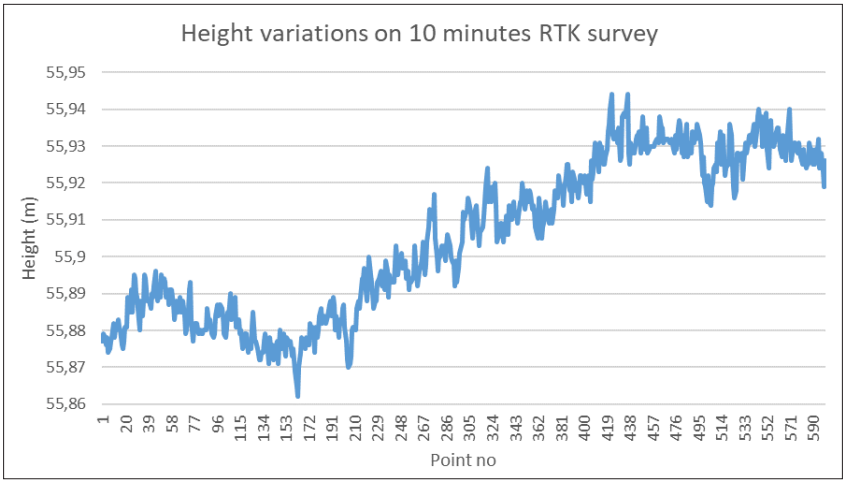

Fig. Height variance on 10 minutes on RTK survey using VRS solution

ASSESSMENT OF ACCURACY OF GNSS MEASUREMENT MODELS USING BASE STATION AND RADIO MODULE SOLUTIONS

Armands Celms[1], Linda Grinberga[1], Toms Lidumnieks[1,2], Jolanta Luksa[1], Miks Brinkmanis-Brimanis[1]

[1] *Latvia University of Life Sciences and Technologies, Liela street 2, Jelgava, Latvia*
[2] *Latvian Geospatial Information Agency, Riga, Latvia*
E-mail: armands.celms@lbtu.lv

Global navigation satellite systems (GNSS) historically been known as one of the newest technologies since the 1970s. GNSS originally developed for military purposes in the USA (GPS – Global Position System). There are several satellite systems in the world. Satellites, International Research Base Stations, regional/national and local base stations form a permanent geodetic frame. Research on the size and shape of the Earth-planet, climate, sea, urban planning. In geodesy, a network of global positioning base stations makes it possible to assess the movements of continents, land plates at international level. GNSS is an important technology in navigation, logistics, economics, land surveying and other "geo" sectors.

GNSS equipment/receivers and their manufacturers are applying new designs and electronics. Initially GNSS instruments used with single frequency signal reception, later expanding the number of GNSS signal channels to two frequencies. Such technological improvements nowadays improve the certainty, reliability and accuracy – the overall quality – of GNSS measurements. The GNSS base station enables the surveyors, other user's GNSS receiver to determine coordinates with an accuracy of two centimeters in real time (RTK) and with an accuracy of five millimeters using the accumulated post-processing data.

Various types of factors hamper GNSS measurements. The GNSS signal (radio wave) travels in airspace, in urban environments and is a physical parameter. Any obstacle – tree, building walls, and atmospheric effect – makes GNSS measurements less accurate. The GNSS signal must be strong and free from attenuation and suppression effects.

This study develops GNSS models that show the comparison, certainty and reliability of GNSS measurements using different types of GNSS techniques. Evaluation of Latvian Global Positioning Reference Station Network – LatPos system measurements against a corresponding RTK solution method using Latvian Global Positioning Network geodetic point (G2 class).

SEISMIC MOMENT TENSOR AND FOCAL MECHANISM OF THE MW3.3 EARTHQUAKE OF MAY 11, 2021 IN THE KYOTO-OSAKA BORDER REGION DETERMINED BY WAVEFORM INVERSION

Dmytro Malytskyy[1], Kimiyuki Asano[2], Miroslav Hallo[2], Andriy Gnyp[1], Oleksandra Astashkina[1], Lucia Fojtikova[3], Jiří Málek[3], Ruslan Pak[1], Vasyl Ihnatyshyn[4,5], Valērijs Ņikuļins[6]

[1] *Carpathian Branch of Subbotin Institute of Geophysics, National Academy of Sciences of Ukraine, 3-b Naukova str., 79060 Lviv, Ukraine*

[2] *Disaster Prevention Research Institute, Kyoto University, Gokasho, Uji, Kyoto 611-0011, Japan*

[3] *Institute of Rock Structure and Mechanics, Academy of Science of the Czech Republic, Prague, Czech Republic*

[4] *Institute of Geophysics, National Academy of Sciences of Ukraine, Kyiv, Ukraine*

[5] *Ferenc Rákóczi II Transcarpathian Hungarian Institute, Kossuth square, 6. 90202 Berehove, Ukraine*

[6] *SIA Geo Consultants Olīvu str. 9, Riga, Latvia*

Email: dmalytskyy@gmail.com

Determining parameters of an earthquake source is an important task for a deeper study of the source processes itself, the calculation of theoretical seismograms at defined sites, a comparative analysis of different approaches in forward and inverse problems, and for the tasks of engineering seismology as well [1]. In the case of weak-to-moderate earthquakes, the polarities and amplitudes of the first arrivals of P-waves observed at seismic stations are usually used to determine the focal mechanism. When there are available observed waveforms at a large number of stations with azimuths evenly distributed around the epicenter and a sufficiently accurate velocity model, the inversion usually results in a satisfactory and precise focal mechanism solution. The problem tackled in this contribution is an inversion of the focal mechanism if a low number of seismic stations is available.

For the purpose of this research, we selected a weak crustal earthquake that occurred on May 11, 2021, on Kyoto-Osaka border in Japan (06:08:44.03 UTC, 34.836°N, 135.616°E, Mw3.3, depth 12.49 km). Three-component waveforms observed by CEORKA (Committee of Earthquake Observation and Research in the Kansai Area) seismic stations are shown in Fig. 1. The seismic moment tensor of the earthquake, shown in Fig. 2, was determined by specialists of the Japanese National Research Institute for Earth Science and Disaster Resilience (NIED) by inverting the whole observed waveforms from three broadband stations F-net.

In the current contribution, we present results of determining the source time function (STF) and moment tensor of the same earthquake using a method for moment tensor inversion of only direct P- and S-waves. The used method is presented in [2, 3], it is a version of the matrix method developed for the calculation of direct waves in horizontally layered medium on a half-space radiated from the point source represented by its moment tensor.

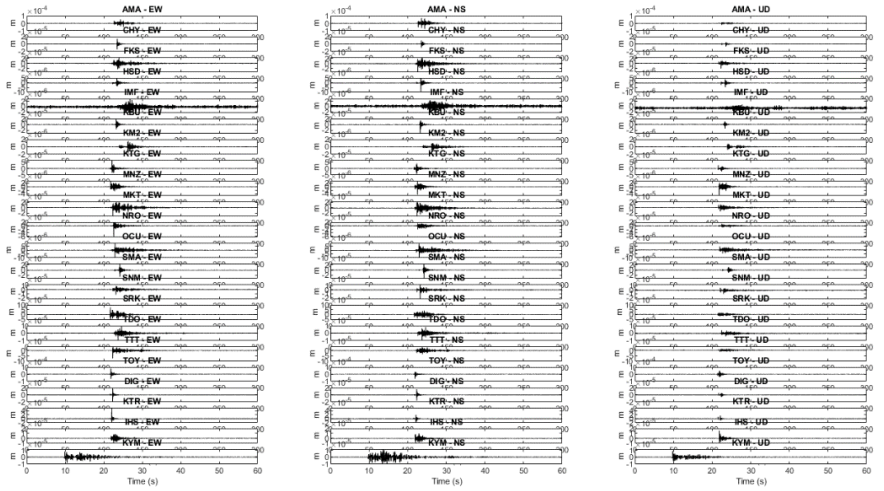

Fig. 1. Records (in displacements) of the Kyoto-Osaka earthquake of May 11, 2021 (data from CEORKA, http://www.ceorka.org/)

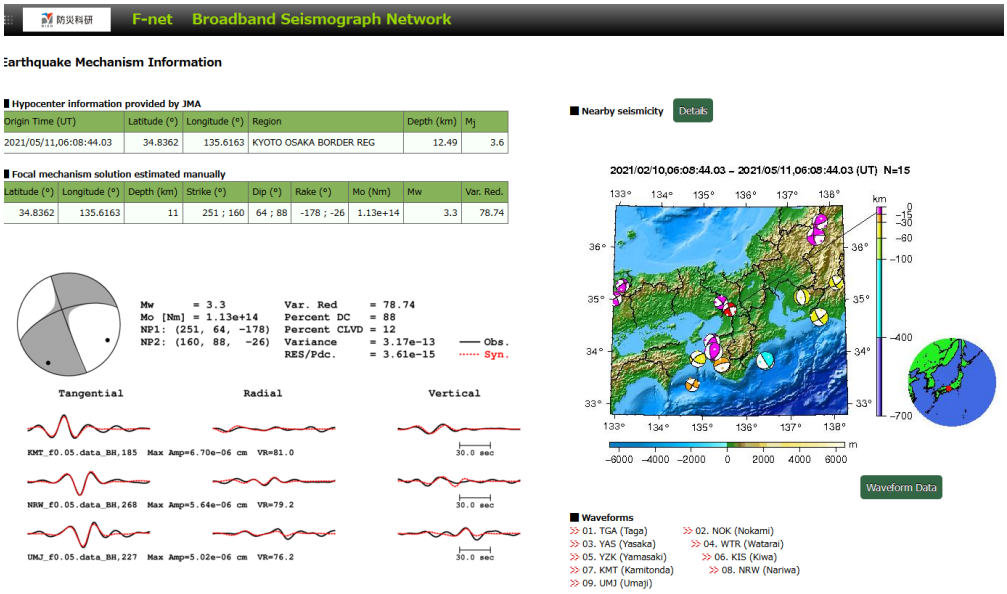

Fig. 2. Focal mechanism of the Kyoto-Osaka earthquake obtained by the seismic moment tensor inversion by NIED F-net (https://www.fnet.bosai.go.jp/event/tdmt.php?_id=20210511060700&LANG=en)

The seismic moment tensor was determined using our method by inverting the waveforms corresponding only to direct waves recorded at four stations: DIG, NRO, OCU, and MNZ (Fig. 3), and eleven stations of the local strong-motion seismological observation network CEORKA: DIG, NRO, OCU, MNZ, TOY, HSD, KM2, KTR, IHS, SMA, and TDO (Fig. 4).

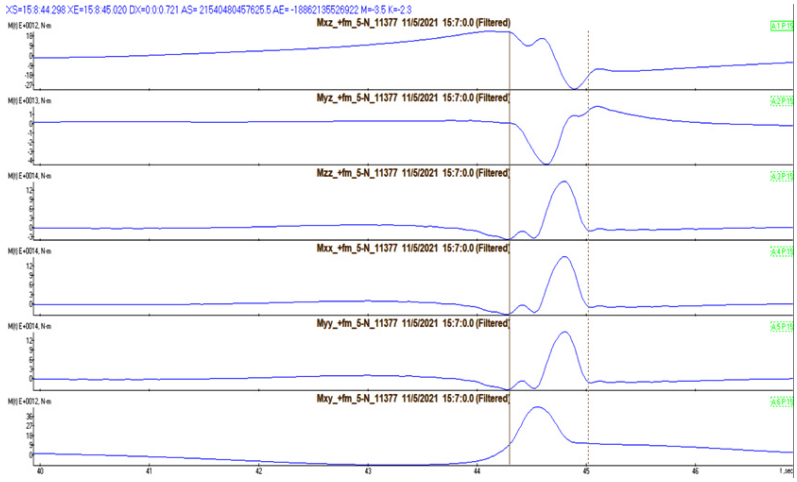

(a)

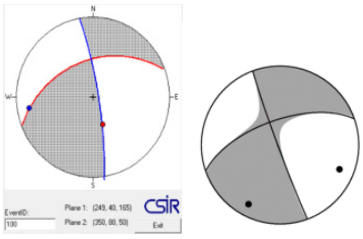

Mw = 3.3
Mo [Nm] = 1.13e+14
NP1: (251, 64, -178)
NP2: (160, 88, -26)

Var. Red = 78.74
Percent DC = 88
Percent CLVD = 12
Variance = 3.17e-13
RES/Pdc. = 3.61e-15

Obs.
Syn.

(b)

Fig. 3. Seismic moment tensor obtained for the 11 May 2021 earthquake by inverting the waveforms of only direct P- and S-waves at four stations (DIG, NRO, OCU, MNZ) (a); the seismic moment tensor released by NIED F-net (b, left), and corresponding to the seismic moment tensor determined by inverting the waveforms of only direct P- and S-waves at the stations DIG, NRO, OCU, and MNZ (b, right)

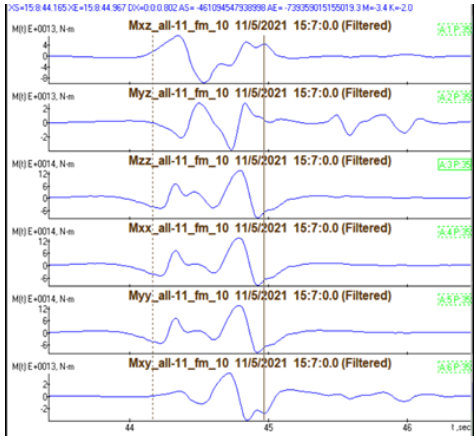

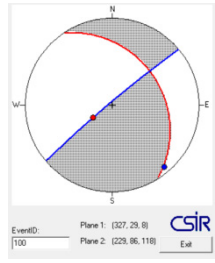

Fig. 4. Seismic moment tensor solution (left) and focal mechanism (right) obtained using records from 11 stations, DIG, NRO, OCU, MNZ, TOY, HSD, KM2, KTR, IHS, SMA, and TDO

To conclude, the seismic moment tensor inversion is important but non-trivial task and the number of observation points influences the precision of the solution. Still, when using appropriate advance technicks and carefull data quality check, it is possible to infer the focal solution from a low number of observational points.

Acknowledgements

This research is a result of the research visit in Japan supported by the Disaster Prevention Research Institute (DPRI) of Kyoto University. In this study, we use earthquake waveforms recorded by seismic stations operated by the CEORKA (Committee of Earthquake Observation and Research in the Kansai Area, http://www.ceorka.org/).

References

[1] Doi, K. The operation and performance of Earthquake Early Warnings by the Japan Meteorological Agency. *Soil Dynamics and Earthquake Engineering*. **2011**, 31, 119–126.

[2] Malytskyy, D. Analytic-numerical approaches to the calculation of seismic moment tensor as a function of time. *Geoinformatika*. **2010**, 1, 79–85 (in Ukrainian).

[3] Malytskyy, D. Mathematical modeling in the problems of seismology. *Naukova Dumka*, *Kyiv*. **2016**, 277 (in Ukrainian).

FEATURES OF TECTONIC STRESS IN THE EASTERN BALTIC REGION

Valērijs Ņikuļins[1], Dmytro Malytskyy[2]

[1] *SIA Geo Consultants Olīvu str. 9, Riga, Latvia*

[2] *Carpathian Branch of Subbotin Institute of Geophysics, National Academy of Science of Ukraine, St. Naukova, 3-b, Lviv, 79060, Ukraine*

E-mail: seismolat@gmail.com

Tectonic stress is an important factor that controls the occurrence of earthquakes. Knowledge of the stressed state of the earth's crust is necessary to understand geodynamic processes, the activation of tectonic faults that are located near energy facilities (nuclear power plants, hydroelectric power plants), the disposal of hazardous environmental waste, including storage facilities for radioactive materials, and underground hydrocarbon storage facilities. Taking into account tectonic stresses allows minimizing the consequences when the regime of anthropogenic loads changes.

Using the *World Stress Map* (WSM) database and supplementing it with information on tectonic earthquakes in the Eastern Baltic region (mainly earthquakes in Estonia [1]), a generalized map of the azimuths of maximum horizontal stresses S_{Hmax} in the East Baltic region and adjacent territories was created (Fig.).

The state of tectonic stress can be assessed using 4 parameters: the orientation S_{Hmax} and three scalar quantities – three principal stresses S_v, S_{Hmax} and S_{hmin}. Depending on the ratios of the three principal stresses, there are three main variants of the earthquake focal mechanisms: *Normal faulting* ($S_V > S_{Hmax}$), *Strike-slip faulting* ($S_{Hmax} > S_V > S_{hmin}$) and *Thrust faulting* ($S_{Hmax} > S_{hmin} > S_v$).

Parameter S_{Hmax} was estimated based on the solution of earthquake focal mechanisms. The method based on solving the earthquake focal mechanisms makes the largest contribution (from 74 to 86 %) to the assessment of direction of S_{Hmax}. In the study area, a minor contribution to the estimating the direction of S_{Hmax} make other methods: *hydraulic fracturing measurement, overcoring or other strain relief measurement, well bore breakout orientation from analysis of individual breakouts.*

All information on the earthquake focal mechanisms and their parameters in the Eastern Baltic region from 1976 to 2018 previously was summarized, i.e. for the instrumental observation period. Complete or partial solutions to earthquake focal mechanisms were analyzed for 8 earthquakes with magnitudes from 1.2 to 5 [2].

Smoothing of the S_{Hmax} directions is performed on a regular grid using a special smoothing algorithm [3]. Directions of S_{Hmax} were calculated using 0.5° grid, with a search radius of 500 km, taking into account data quality. With this long-wave averaging method, first of all, the influence of large-scale terrestrial structures is taken into account, while the influence of local inhomogeneities is less noticeable.

Data quality had four accuracy class from A to E. The accuracy class determines the deviation of the azimuth S_{Hmax} from its average value. Class A corresponds to a deviation of ± 15°, Class B: ± 20°, Class C: ± 25°, Class D: ± 40°, and Class E corresponds to a deviation > ± 40°.

The azimuths of tectonic stresses S_{Hmax} in the Eastern Baltic region have a number of features.

Azimuth of S_{Hmax} decreases from 157°–166° in the Kaliningrad region to 102°–114° in Estonia. On the territory of Latvia, azimuths S_{Hmax} vary from 115° to 150°.

The predominant type of earthquake focal mechanisms in the Eastern Baltic region are *Strike-slip* and *Reverse*.

Within the Baltic Syneclise, a certain influence of the thickness of the sedimentary cover on the azimuth S_{Hmax} was revealed. With an increase in the thickness of the sedimentary cover (from 0.25 km in Estonia to 2.1 km in the Kaliningrad region of Russia), the azimuth S_{Hmax} increases.

Individual deep tectonic faults in the earth's crust can influence on changes in S_{Hmax} azimuths. In particular, after the *Taurage-Ogre* deep fault, the azimuth S_{Hmax} begins to decrease from 170° to 90° and then increases slightly again to 104°. Thus, the effect of rotation of the S_{Hmax} vectors is noted. However, not all deep tectonic faults have such a significant effect on changes in S_{Hmax} azimuths.

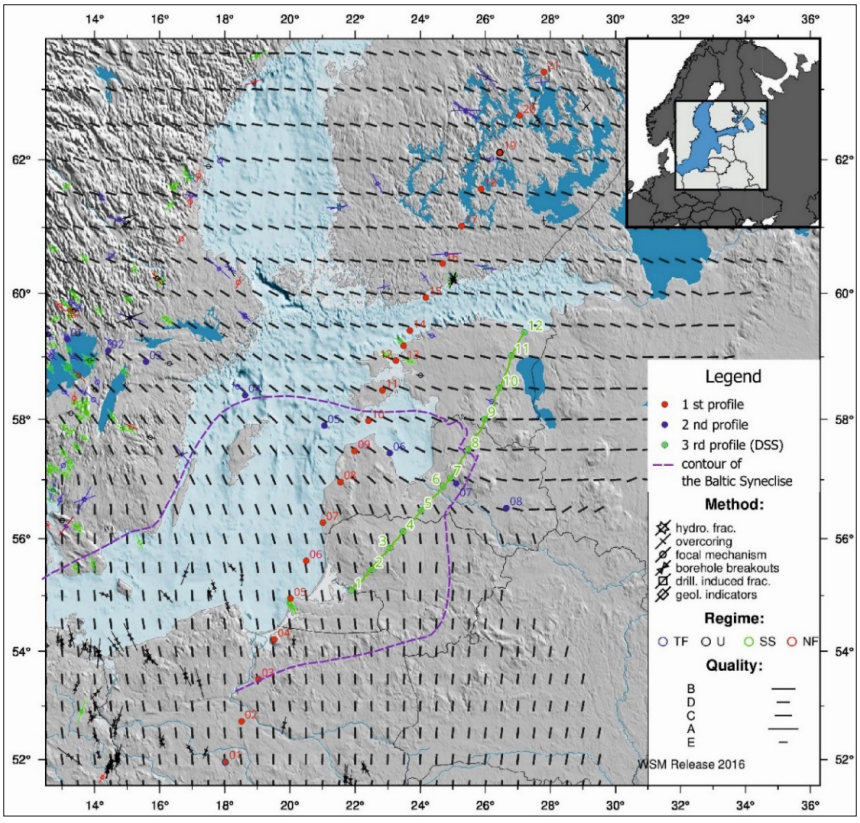

Fig. Generalized Map of maximum horizontal stresses S_{Hmax} vectors in the Eastern Baltic region and surrounding territories

Comments: red color – points on profile 1, blue color – points on profile 2, green color – 1986 DSS profile and points on the profile, the purple dotted line shows the outline of the Baltic Syneclise.

A connection was discovered between the azimuth S_{Hmax} and the gravitational influence [4] of individual parts of the earth's crust along the *Deep Seismic Sounding* (DSS) profile. The maximum correlation coefficient was found between the azimuth S_{Hmax} and the gravitational influence of the sedimentary cover (k = – 0.85), the gravitational influence of the earth's crust without taking into account the influence of the sedimentary cover and the upper part of the basement (k = 0.84), the gravitational influence of the thickness of the earth's crust up to boundary IV (k = 0.83).

The results of assessing the azimuths of maximum horizontal stresses S_{Hmax} in the Eastern Baltic region are important from scientific and practical points of view.

From a scientific point of view, knowledge of compression and extension areas will allow to better understand the history of the geodynamic development of the region.

From a practical point of view, knowledge of azimuths and S_{Hmax} values will make it possible to assess the geodynamic potential in the area of important engineering and technical facilities. For example, this is necessary at the *Plavinu* hydroelectric power station, in the area of the underground gas storage facility in *Incukalns*. Assessment of tectonic stress parameters may be relevant for understanding the geodynamic conditions in the areas where radioactive materials are buried in *Baldone* and *Ignalina*, as well as in the area of nuclear power plants located near the East Baltic region (Leningrad, Belarusian).

The next stage of research is to estimate the magnitudes (scalar quantities) of three principal stresses: S_V, S_{Hmax} and S_{hmix}, that is important for modeling geodynamic conditions and estimation of geodynamic potential in the area of the above objects.

References

[1] Soosalu, H.; Uski, M.; Komminaho, K.; Veski, A. Recent Intraplate Seismicity in Estonia, East European Platform. *Seismological Research Letters*. **2022**, 93, 1800–1811.

[2] Ņikuļins, V.; Malytskyy, D. Review of parameters and focal mechanisms of modern earthquakes of Eastern Baltic region. *Latvijas Universitāte 82.zinātniskā konference. Lietišķa ģeoloģija.* **2024**, https://www.geo.lu.lv/fileadmin/user_upload/lu_portal/projekti/gzzf/Konferences/82_KONF_2024/vaerijs-nikulins-1.pdf.

[3] Müller, B.; Wehrle, V.; Hettel, S.; Sperner, B.; Fuchs, F. A new method for smoothing oriented data and its application to stress data. *In: M Ameen (ed) Fracture and in situ stress characterization of hydrocarbon reservoirs*. **2003**, v. 209. *Special Publication: Geological Society, London*. 107–126.

[4] Ozolinya, N.K.; Kovrigin, V.P. Report on the topic "Generalization of the physical properties of rocks on the territory of the Latvian SSR" for 1984–1986. **1986**. *Geology Department of the Latvian SSR*, KGE, 1, 144. (In Russian).

SEISMOLOGICAL MONITORING OF LATVIA – NECESSITY, COMPLEXITIES AND FUTURE PROSPECTS

Viesturs Zandersons, Jānis Karušs

University of Latvia, Faculty of Geography and Earth Sciences, Jelgavas str. 1, Riga, Latvia
E-mail: viesturs.zandersons@lu.lv

Seismological monitoring is crucial for understanding and mitigating the effects of earthquakes and related geophysical phenomena. Globally, the importance of seismological monitoring is related to devastating earthquakes in tectonically active regions, which often lead to massive loss of life and destruction of infrastructure, as well as nuclear non-proliferation, where seismology in particular plays a key role on worldwide monitoring of nuclear weapon tests [1, 2]. However, seismological monitoring is important even in relatively inactive, low-seismicity areas, such as Latvia, due to presence of small-magnitude natural earthquakes and human induced seismic activities [3]. Here we outline main necessity for local seismic wave monitoring in Latvia, its aims and scope as well as most important challenges and prospects for seismological measurements in the Baltic region.

Baltic region is characterized by relatively low seismic activity. In the recent history, no earthquakes larger than magnitude five have been observed, with largest ones occurring in 1976 in Osmussaare, Estonia with magnitude 4.7 and in 2004, Kaliningrad region, with

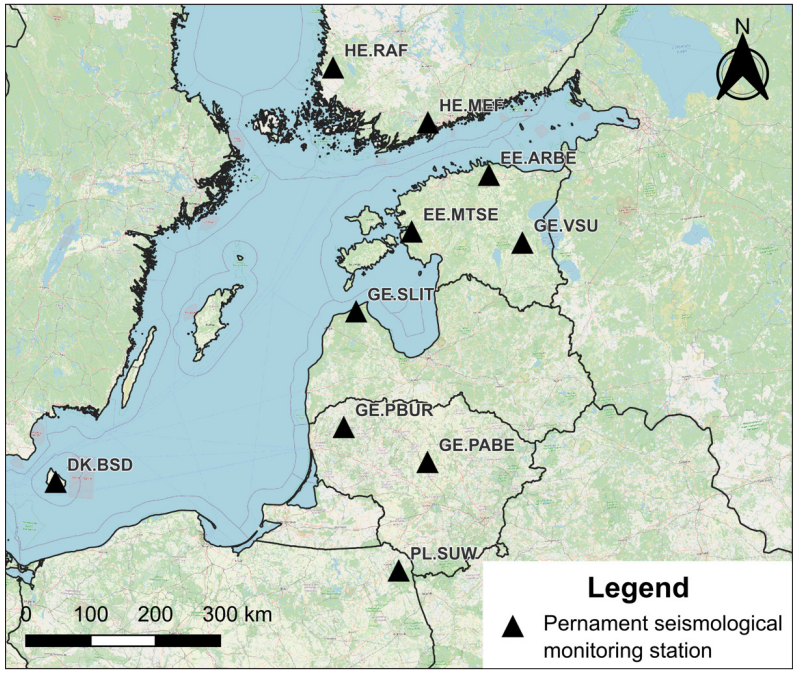

Fig. 1. Seismological observation stations around Latvia

magnitudes reaching 5.2 [4, 5]. Nevertheless, there are multiple small magnitude (<2.5) events observed with almost annual return frequency [3, 6]. In addition, seismic vibrations from human made blasts, either from mining of natural resources or military drills are commonly observed in the area. The area is monitored by a virtual network of 10 permanent broadband seismic stations – three in Estonia, two – Lithuania, two – Finland, one in Poland, Latvia and Denmark (Fig. 1). While existing stations are used successfully to monitor large earthquakes, a more intricate network is required to accurately locate smaller events [3, 6], which can be crucial when calculating the seismic hazards.

Main challenges of seismological observation in Latvia are thus related to lack of seismic observation stations and lack of manpower for in-depth seismic data processing. The lack of observation stations is highlighted by a recent seismic event in the morning of 30th April 2024. Multiple people reported ground shaking in a relatively large region for more than 10 seconds in Courland, Latvia to maximum intensity of 4 by EMS-98 scale, the description of movement being similar to a shallow earthquake. However, as no seismic stations were nearby, with the closest one being more than 80 km away, signs of an event were detected in only one – Slītere – observation station. This greatly complicated the analysis of the event. The location could be determined by only back-azimuth from the mentioned observation station, and the precise P and S arrivals were masked by relatively large background noise. This led to epicenter location in the Baltic Sea, not matching the shaking reported by people (Fig. 2).

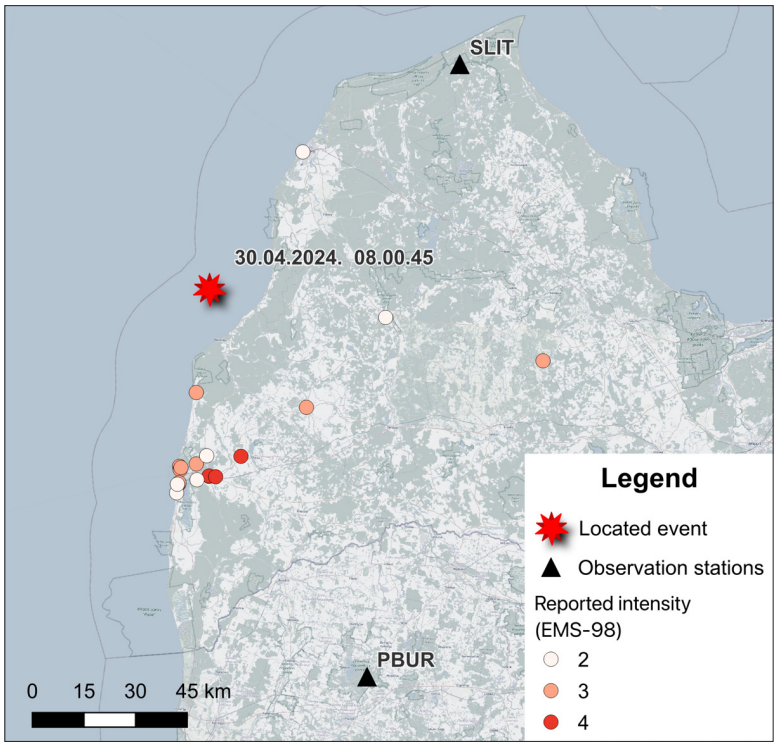

Fig. 2. Event analysis and reported intensity of the event on the morning of 30th April 2024

In-depth seismic monitoring using a sparse station network also takes significant amount of time, as advanced methods such as station cross-correlation must be used to determine even bare minimum information – first P and S arrivals. In fact, the recent testing of machine-learning (ML) algorithms in event detection highlighted many cases that have been missed by routine analysts, likely due to lack of manpower in the monitoring network [7].

It is very likely that the importance of seismic monitoring in Latvia will only increase. Large scale infrastructure projects related to the use of geological resources such as deep mining or underground CO_2 storage will necessitate improved ground monitoring, considering environmental risks. Seismic monitoring can also play a crucial role in geopolitics, an example being the recent destruction by blasting of the Nordstream pipeline in the Baltic Sea. In future, improvements in the seismological observing network, and data processing are required. Recent work regarding ML methods in seismic monitoring is a good start, however more emphasis needs to be put on ML model adjustment. In addition, seismic event parameter analysis is also a topic that needs attention, which could directly lead to improved seismic hazard analysis in the region.

References

[1] CTBTO. Ending Nuclear Tests https://www.ctbto.org/our-mission/ending-nuclear-tests (accessed May 21, 2024).

[2] Bormann, P. Chapter 1: History, Aim and Scope of the 1st and 2nd Edition of the IASPEI New Manual of Seismological Observatory Practice. *New Man. Seismol. Obs. Pract. 2 NMSOP-2*, **2013**. https://doi.org/10.2312/GFZ.NMSOP-2_CH1.

[3] Ņikuļins, V. G. Seismological Monitoring in Latvia. *Summ. Bull. Int. Seismol. Cent.*, **2020**, *54* (I), 50–66. https://doi.org/10.31905/BKETRT2R.

[4] Gregersen, S.; Wiejacz, P.; Dębski, W.; Domanski, B.; Assinovskaya, B.; Guterch, B.; Mäntyniemi, P.; Nikulin, V. G.; Pacesa, A.; Puura, V.; et al. The Exceptional Earthquakes in Kaliningrad District, Russia on September 21, 2004. *Phys. Earth Planet. Inter.*, **2007**, *164* (1–2), 6374. https://doi.org/10.1016/j.pepi.2007.06.005.

[5] Nikonov, A.A; Sildvee, H. Historical Earthquakes in Estonia and Their Seismotectonic Position. *Geophysica*, **1991**, *27* (1–2), 79–93.

[6] Soosalu, H.; Uski, M.; Komminaho, K.; Veski, A. Recent Intraplate Seismicity in Estonia, East European Platform. *Seismol. Res. Lett.*, **2022**, *93* (3), 1800–1811. https://doi.org/10.1785/0220210277.

[7] Zandersons, V.; Karušs, J.; Brants, M. Automatic Induced Seismic Event Detection in Low Seismicity Areas. In *28th IUGG General Assembly Berlin. Conference proceedings*; Berlin, 2023.

ON ACCURACY OF VERTICAL DEFLECTION MEASUREMENTS BY DIGITAL ZENITH CAMERA VESTA

Ansis Zariņš, Inese Vārna, Augusts Rubāns

University of Latvia, Institute of Geodesy and Geoinformatics, Jelgavas str. 3, Riga, Latvia
E-mail: ansis.zarins@lu.lv

In order to obtain estimates of stability and statistical properties of deflection of vertical (DoV) measurements by digital zenith camera VESTA [1, 2], 26 overnight (typically 7–12 hours long) observation sessions were done at a fixed site by two adjacent cameras (placed within 1–10 meters from each other). About 5000 measurement positions for each instrument were abtained. 12-position (sub-session duration of 15–20 minutes) DoV solutions [1, 2] were calculated within a sliding data window along these positions. Analysis of data showed the following:

- On average, DoV values obtained by both instruments are quite close (Fig. 1), difference between averages (vertical lines on Fig. 1 B, C) is 0.01 arc seconds for X (η) and 0.024 arc seconds for Y (ξ) at distribution rms around 0.12 arc seconds. Nevertheless, these differences are not negligible in comparison to formal accuracy estimate (RMS/sqrt(N)) of ~0.002 arc seconds.

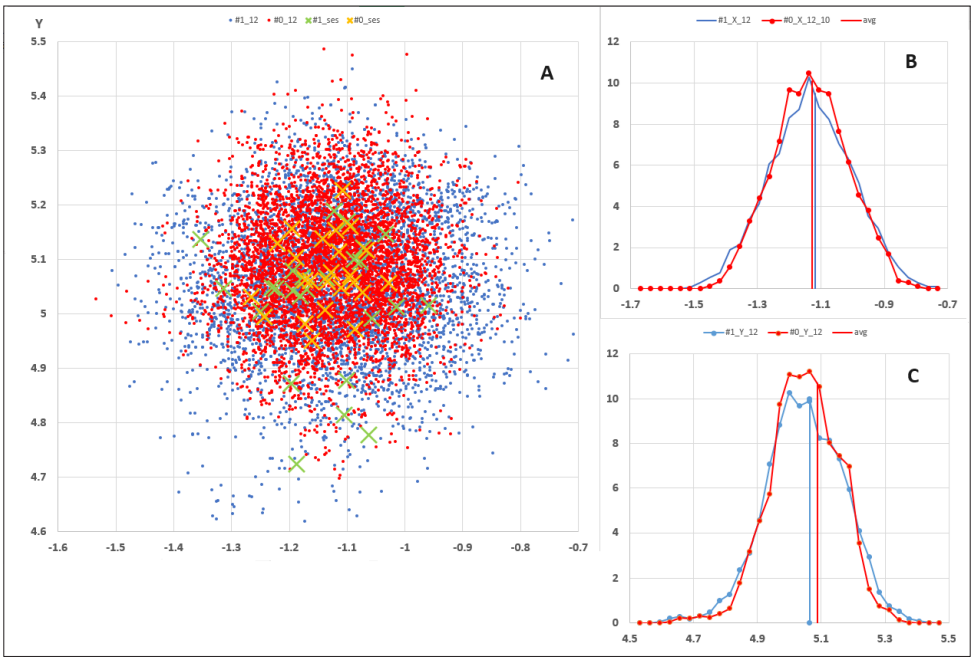

Fig. 1. Distribution of 12-position DoV values (in arc seconds) obtained by two adjacent instruments: A – scatter on XY plane, B – histogram of X (η) component variations, C – histogram of Y (ξ) component variations

Distributions of DoV values for different sizes of sliding data window are quite similar; most extreme values are gradually eliminated for data windows of more duration, leading to slightly smaller RMS (Fig. 2). Averages of individual sessions (slanted crosses on Fig. 1A) may differ from total (many sessions) average by up to ~0.2 arc seconds (Fig. 1).

- Although distribution of results both for individual sessions and for whole bulk of data look close to normal, averages of individual simultaneous sessions show considerable differences (occasionaly up to 0.2 arc seconds) between both instruments.
- Within a session, random-looking fast variations (with periods of minutes) are superimposed on others, much slower (with periods of hours to days), but in the long run also random (Fig. 3). These variations presumably are result of varying horizontal gradients of atmosphere refractivity (density).
- No persistent dependency on time-in-day (UT) was found.
- Contrary to expectatations, close correlation of results of adjacent cameras was not found. Differences in DoV components are considerable, up to several tenths of arc second. Time dependency of differences include both fast and slow components. However, quite often similar time dependency patterns are present, also both fast and slow. That indicates presence of several variability mechanisms, some common to both instruments and some separate.
- No pronounced dependency on distance between cameras (within ~1 to 10 m).
- Attempts to provoke more intense air turbulence in direct proximity of cameras (heaters, fans) led to slightly bigger variability of results, but did not change general pattern.

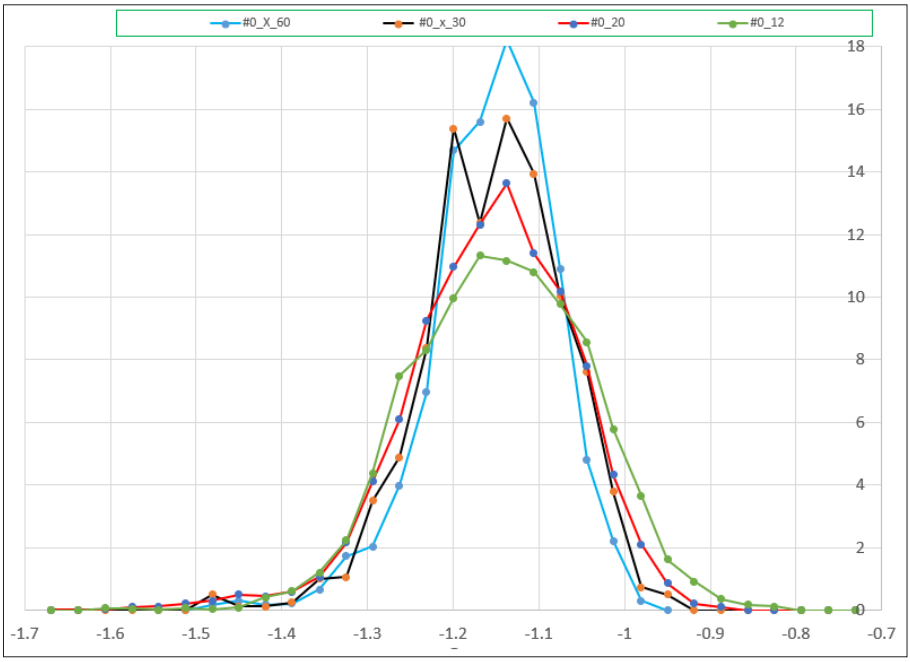

Fig. 2. Distribution of DoV X (η) value for different sizes of sliding data window (60, 30, 20 and 12 rotation positions)

Presently we find it difficult to propose detailed explanations of such behavior. Some differences between cameras may arise inside telescope assemblies. Fast twinkling component, caused by passing of turbulece cells across field of view, most probably is similar for both cameras, but is far beyond time resolution of DoV solutions (not less then a few minutes). Structure and dynamics of horizontal density gradients in atmosphere are poorly known, but, as it seems, should not experience big differences between cameras, especially in far zone. Possibly local topography features add some input. Additionl research would be necessary to clarify situation.

References

[1] Zariņš, A.; Rubans, A.; Silabriedis, G. Digital zenith camera of the University of Latvia. *Geodesy and Cartography.* **2016**, 42 (4), https://doi.org/10.3846/20296991.2016.1268434.

[2] Zariņš, A.; Rubans, A.; Silabriedis, G. Performance analysis of Latvian zenith camera. *Geodesy and Cartography.* **2018**, 44 (1), https://doi.org/10.3846/gac.2018.876.

A TEST OF HEIGHT TRANSFER USING DIGITAL ZENITH CAMERA VESTA AND GNSS MEASUREMENTS

Inese Varna[1], Ansis Zarins[1], Gunars Silabriedis[1], Katerina Morozova[1], Armands Celms[2]

[1] *University of Latvia, Institute of Geodesy and Geoinformatics, Jelgavas str. 3, Riga, Latvia*
[2] *Department. of Land Management and Geodesy, Latvia University of Life Sciences and Technologies, Akademijas str. 11, Jelgava, Latvia*
E-mail: inese.varna@lu.lv

Geometric leveling is a conventional method for transferring height differences between points in a leveling network relative to the sea-level surface, or geoid. However, this approach is labor-intensive and time-consuming, particularly over long distances or in the presence of topographic or administrative barriers.

An alternative to geometric levelling involves using precise geoid undulation data, denoted as N, along with ellipsoidal GNSS heights, denoted as h, to derive normal or orthometric height, H = h – N. While this method offers faster and easier height determination, it's hindered by the limited accuracy of geoid surface properties necessary for precise leveling. Deflection of vertical measurements, indicating the geoid surface's inclination with respect to the reference ellipsoid surface, along a traverse between leveling points, present a viable solution. These measurements can be obtained independently for intermediate points, and a combination of old and new data can be used, allowing for significantly larger distances between measurement points compared to geometric leveling.

Measurements of deflection of vertical conducted using digital zenith cameras have been employed in studies to determine geoid undulation, as evidenced by works such as those by Hirt and Flury (2008) [1], Voigt and Denker (2014) [2], and Schack et al. (2018) [3]. In the United States, numerous surveys aimed at validating geoid slope along the traverse have been undertaken over time, employing various methods and technologies, as documented in studies by Smith et al. (2013) [4], Wang et al. (2017) [5], and van Westrum et al. (2021) [6].

This study conducted a trial of height transfer using quasi-geoid undulation extrapolation. The approach combined deflection of vertical measurements from the digital zenith camera VESTA (Vertical by STArs) with ellipsoidal height measurements obtained via GNSS. To evaluate this approach, extensive deflection of vertical measurements were collected along a 4.5-kilometer traverse between first-order leveling points. GNSS height measurements were taken at three first-order leveling points situated at each end of the traverse and in the midpoint. Subsequently, the height transfer outcomes were compared with the existing network data sourced from the national geodetic database.

Utilizing extrapolation techniques, geoid undulation along a traverse with either measured or known deflection of vertical values can facilitate precise transfer of undulation variations. When combined with GNSS ellipsoidal height measurements, this method enables accurate transfer of heights above sea level.

The accuracy of geoid undulation transfer can reach approximately 0.1 mm/km or higher, given a deflection of vertical accuracy of around 0.1 arcseconds and an average spacing

between measurement points of a few hundred meters. In areas with relatively uniform geoid surfaces, the spacing between points can be extended, potentially up to 1–2 km. However, in regions with complex topography, such as mountainous terrain, closer point spacing may be necessary, and the selection of points should consider the impact of topographic features.

If a lower accuracy (1–2 mm/km) is acceptable, a global geopotential model with high spatial resolution, such as GGMplus, may suffice, with potential support from deflection of vertical measurements calibration. Nonetheless, simultaneous calculations utilizing geoid model data can help identify major data inaccuracies.

Combining deflection of vertical measurements with GNSS-measured ellipsoidal heights for determining normal height presents several advantages over geometrical leveling. deflection of vertical and ellipsoidal height measurements can be independently obtained for intermediate points, allowing for the integration of old data with new measurements. This approach proves advantageous for long-distance profiles or when encountering natural or administrative obstacles. GNSS measurements can be conducted concurrently or sequentially with deflection of vertical measurements, offering flexibility in measurement scheduling based on weather conditions and equipment availability. Furthermore, the distance between measurement points can be significantly larger compared to geometrical leveling.

The deflection of vertical measurement process with digital zenith camera VESTA is completely automated and can be conducted by a single operator, whereas geometrical leveling campaigns are resource-intensive, necessitating a team of skilled individuals and inflating campaign expenses. However, deflection of vertical measurements are restricted to clear nights, posing challenges when scheduling measurements in regions with frequent cloud cover, although geometric leveling also demands specific weather conditions. Thus, the suggested method could present a more cost-effective and convenient option compared to traditional geometrical leveling.

References

[1] Hirt, C.; Flury, J. Astronomical-Topographic Levelling Using High-Precision Astrogeodetic Vertical Deflections and Digital Terrain Model Data. *J. Geod.* **2008**, https://doi.org/10.1007/s00190007-0173-x.

[2] Voigt, C.; Denker, H. Validation of Second-Generation GOCE Gravity Field Models by Astrogeodetic Vertical Deflections in Germany. In *International Association of Geodesy Symposia*.**2014**, https://doi.org/10.1007/978-3-642-37222-3__38.

[3] Schack, P.; Hirt, C.; Hauk, M.; Featherstone, W. E.; Lyon, T. J.; Guillaume, S. A High-Precision Digital Astrogeodetic Traverse in an Area of Steep Geoid Gradients Close to the Coast of Perth, Western Australia. *J. Geod.* **2018**, https://doi.org/10.1007/s00190-017-1107-x.

[4] Smith, D. A.; Holmes, S. A.; Li, X.; Guillaume, S.; Wang, Y. M.; Bürki, B.; Roman, D. R.; Damiani, T. M. Confirming Regional 1 Cm Differential Geoid Accuracy from Airborne Gravimetry: The Geoid Slope Validation Survey of 2011. *J. Geod.* **2013**, https://doi.org/10.1007/s00190-013-0653-0.

[5] Wang, Y. M.; Becker, C.; Mader, G.; Martin, D.; Li, X.; Jiang, T.; Breidenbach, S.; Geoghegan, C.; Winester, D.; Guillaume, S.; Bürki, B. The Geoid Slope Validation Survey 2014 and GRAV-D Airborne Gravity Enhanced Geoid Comparison Results in Iowa. *J. Geod.* **2017**, *91*, 1261–1276, https://doi.org/10.1007/s00190-017-1022-1.

[6] van Westrum, D.; Ahlgren, K.; Hirt, C.; Guillaume, S. A Geoid Slope Validation Survey (2017) in the Rugged Terrain of Colorado, USA. *J. Geod.* **2021**, *95*, 9, https://doi.org/10.1007/s00190-02001463-8.

GNSS DENIED NAVIGATION USING THE GEOMAGNETIC FIELD

Reinis Lazda, Antra Asare, Oskars Rudzitis, Florian Gahbauer, Mona Jani and Marcis Auzinsh

Laser Centre, University of Latvia, Jelgavas street 3, LV-1004, Riga, Latvia
E-mail: reinis.lazda@lu.lv

High sensitivity magnetometry can be used for various application with respect to the Earth's magnetic field, such as magnetic anomaly detection and navigation using precise measurements of the Earth's magnetic field. Models of the Earth's magnetic field distribution exist, they can be used to determine the necessary magnetic field sensitivity for navigation purposes, see Fig. 1. The magnetic field of the Earth varies in the range of 25 000 to 65 000 nT. Typical magnetic anomaly detection requires a magnetic field sensitivity of less than 10 nT/Hz$^{1/2}$.

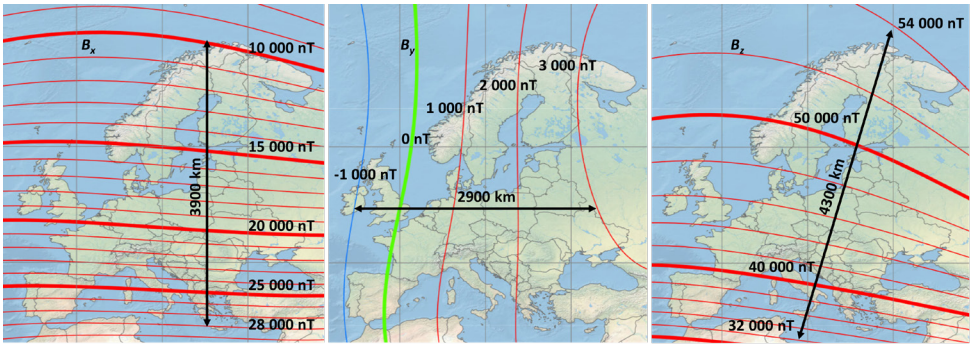

Fig. 1. Earth's magnetic field distribution over Europe [1], approximate change of each magnetic field component – B_x: 4.6 nT / 1 km, B_y: 1.4 nT / 1 km, B_z: 5.1 nT / 1 km

One possible candidate for high sensitivity magnetic field measurements are NV centers in diamond whose quantum properties can be leveraged for magnetic field sensing, additionally the crystal lattice structure of a diamond naturally enables vector magnetometry due to the four possible directions that the NV centers can be oriented in the diamond [2], see Fig. 2. Left. The current magnetic field sensitivity of our experiment using a double quantum ODMR method [3] for slowly varying magnetic fields is on the order of 1 nT/Hz$^{1/2}$, see Fig. 2. Right.

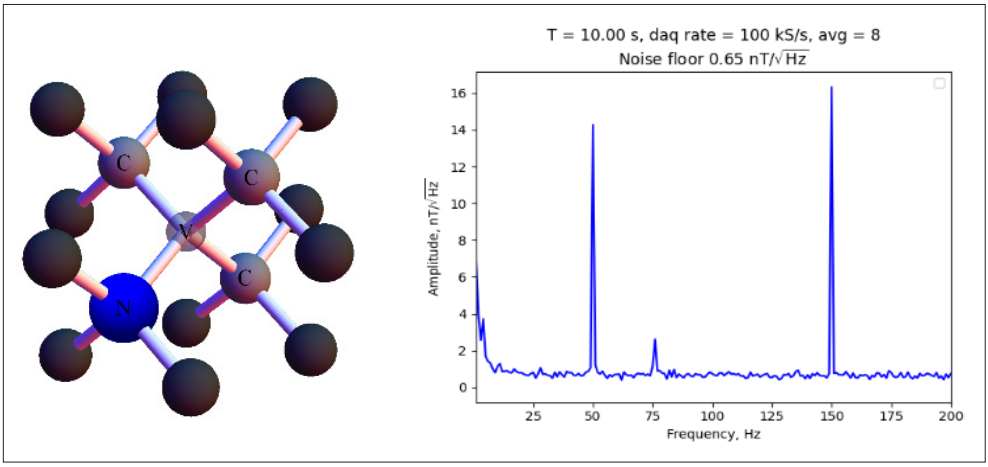

Fig. 2. Left: diamond crystal unit cell with an NV center. Right: experimental PSD noise floor

References

[1] https://www.ncei.noaa.gov/products/world-magnetic-model

[2] Schloss, J. M.; Barry, J. F.; Turner, M. J.; Walsworth, R. L. Simultaneous Broadband Vector Magnetometry Using Solid-State Spins. *Phys. Rev. Applied.* **2018**, 10, 034044.

[3] Fescenko, I.; Jarmola, A.; Savukov, I.; Kehayias, P.; Smits, J.; Damron, J.; Ristoff, N.; Mosavian, N.; Acosta, V. M. Diamond magnetometer enhanced by ferrite flux concentrators. *Phys. Rev. Research.* **2020**, 2, 023394.

MODEL PREDICTIVE CONTROL FOR AUTONOMOUS FLIGHTS OF DRONES – MATHEMATICAL MODELS, SYSTEM DEVELOPMENTS AND TESTS

Felix Vortisch[1, 2], **Reiner Jäger**[1, 2]

[1] *University of Applied Sciences Karlsruhe, Moltkestraße 30, Karlsruhe, Germany*
[2] *Laboratory for GNSS and Navigation, Moltkestraße 30, Karlsruhe, Germany*
E-mail: fe.vortisch97@web.de

The presentation is dealing with the development, simulations and tests of a Model Predictive Control (MPC) flight control for the autonomous flight of configurable drones along a defined trajectory.

The computation of the control parameters $\mathbf{u}(t)$ – e. g. the propeller rotation rates of a propeller drone – is theoretically based on the availability of the full so-called 19 parameter control deviation $d\mathbf{y}(t) = \mathbf{y}(t)_{des} - \mathbf{y}(t)_{nav}$ (nav = multisensory navigated) due to the below mentioned differential equations of flight physics. In case of a remote control, $d\mathbf{y}(t)$ is directly read form the slider-/joystick-based control settings of the pilot. Here the PID control has become a standard to compute continuously the control variables $\mathbf{u}(t)$ at any time t_i.

To fly however autonomously along a desired, in first instance only waypoint-based defined trajectory $\bar{\mathbf{y}}(t)_{des}$, the PID control algorithm becomes inappropriate, as the desired navigation state parameters $\bar{\mathbf{y}}(t)_{des}$ contains 19 parameters. The associated desired way position polygon $\mathbf{y}(t)_{des}$ is however only a 3D sub-vector of $\mathbf{y}(t)_{des}$. So there is an large uncertainty, how to "fill up" the missing parameters $\mathbf{y}(t)_{des,\,rest}$, complementary to $\bar{\mathbf{y}}(t)_{des}$, in order be able to solve the differential equation for getting $\mathbf{u}(t)$. This goes hand in hand with the fact that "any" defined trajectory $\mathbf{y}(t)_{des}$ is not guaranteed to be flyable, means controllable, due to the physical characteristics of the inertia matrix J and the motor allocation matrix **M**. **M** is giving the relation (linear in case of propeller drone) between the above controls u(t) and the resulting thrusts and torques in body frame of the drone within the differential equation below. [2]

The MPC avoids all above complications in an autonomous flight. Common with the PID control, the MPC algorithm is based on the unique first order flight physics differential equation $\dot{\mathbf{y}}(t) = \mathbf{f(y(t), J, M, u}(t))$ of a flight object to be controlled. The total vector $\mathbf{u}(t) = [\mathbf{u}(t_1), .., \mathbf{u}(t_j), .. \mathbf{u}(t_m)]$ of the control parameters is in the MPC case piecewise predicted along the desired waypoint trajectory $\bar{\mathbf{y}}(t)_{des}$ in terms of MPC sequences $\mathbf{u}(t_1)$ over control horizons $\Delta T_j = [t_1, .., t_i, .. t_n]j$, $j = 1, n_j$ in time spans ΔT_j. So it holds for the total control vector $\mathbf{u}(t) = \mathbf{u}(t_1), .., \mathbf{u}(t_j), .., \mathbf{u}(t_m)]$. The above-mentioned uncertainties on the complementary parameters $\mathbf{y}(t)_{des,\,rest}$ can be overcome by the MPC method, as well as the problem of flyability of a defined trajectory $\mathbf{y}(t)_{des}$, in respect to get a complete set of unique control parameters $\mathbf{u}(t) = [\mathbf{u}(t_1),.., \mathbf{u}(t_j),.. \mathbf{u}(t_m)]$ along $\mathbf{y}(t)_{des}$. [2]

In the first part of the presentation, the principle of the MPC algorithm is explained, by the derivation of the mathematical model for the computation of sets of controls $\mathbf{u}(t_j)$ over predicted time-horizon ΔT_j. The solution for (t_j) leads to the introduction of a quadratic cost function, which has to be minimized to receive the controls $\mathbf{u}(t_j)$. The MPC method leads to

a $\mathbf{Q}_i$-weighted result with theoretical residuals d$\mathbf{y}$(t) between the controlled and the desired $[\mathbf{y}(t_1)_{des}, .., \mathbf{y}(t_i)_{des}, .., \mathbf{y}(t_{n_j})_{des}]_j$, j = 1, n_j and so in $[\bar{\mathbf{y}}(t_1)_{des}, .., \bar{\mathbf{y}}(t_i)_{des}, .., \bar{\mathbf{y}}(t_{n_j})_{des}]_j$, j = 1, n_j over each time horizon ΔT_j. Further residuals d$\mathbf{y}$(t)´ between the desired $y(t)_{des}$ and the navigated $\mathbf{y}(t)_{nav}$ have to be handled from time to time. In the MPC algorithm the matrices **J** and **M** are set as free configurable parameters, so any type of drones can be configured.

The final part of the presentation is dealing with the implementation of the MPC flight control using python and ACADOS toolkit [1]. The implementation of the MPC flight control is validated and tested under simulation conditions by hardware in the loop (HIL) and software in the loop (SIL). The performance and robustness have been tested and discussed, and the validated MPC flight control system has been adapted for a real-world application.

References

[1] Falanga, D., Foehn, P., Lu, P. and Scaramuzza, D. PAMPC: Perception-Aware Model Predictive Control for Quadrotors. *IEEE/RSJ International Conference on Intelligent Robots and Systems (IROS).* **2018**.

[2] Jäger, R. Geodäten erobern den Luftraum. *DVW-Seminar.* **2019**.

ON THE MOVEMENT OF GPS POSITIONING DISCREPANCY CLOUDS

Jānis Balodis, Madara Normanda, Ansis Zariņš

University of Latvia, Institute of Geodesy and Geoinformatics, Jelgavas str. 3, Riga, Latvia
E-mail: janis.balodis@lu.lv

The geomagnetic storm on March 17, 2015, had a strong impact on the GNSS positioning results in many Continuously Operating Reference Stations (CORS) in Europe. This storm is named St. Patrick's Day storm and it was the first super geomagnetic storm during the 24th Solar Cycle. It gained the attention of many researchers [1–6].

The analysis of Global Positioning System (GPS) observations in Latvian CORS stations discovered a strong impact of this space weather event over the whole country. The impact appeared as a moving cloud of positioning discrepancies across the country. However, the analysis of the days before and after March 17 revealed other smaller duration ionospheric scintillation events daily.

In space weather research the investigations of ionospheric storm effects are of a fundamental importance [6]. By some authors is noticed that the impact is more severe at high latitudes, while at low latitudes the impact is associated with different types of ionospheric disturbance. By contrast, midlatitude irregularities are less severe, and they are usually attributed to expansion of auroral and/or equatorial irregularities under disturbed conditions [6]. The objective of our study was to analyze the GPS positioning discrepancy cloud movement, the Total Electron Content (TEC) and the Rate of Change of TEC Index (ROTI) relationships, as well as discrepancy statistics in mid-latitute region, Latvia.

First, the post-processing of the selected dataset in the Bernese GNSS Software v5.2 [7] was carried out during the contract work of the European Space Agency (ESA) in 2020. Computing strategy parameters included kinematic double-difference network solution, ionosphere-free linear combination, CODE products, and four IGS/EPN network stations (LAMA (Olsztyn, Poland), METS (Metsahovi, Finland), VIS0 (Visby, Sweden), VLNS (Vilnius, Lithuania)) as reference stations. GPS observation data with an elevation cut-off angle of 15° were used for 90 second (sampling data 30 sec) intervals of kinematic post-processing. The FES2004 ocean tidal model was used, along with correction of the solid Earth tide effect. The Dry Global Mapping Function (DRY-GMF) was used for the tropospheric delay modelling. The maximum size of accepted cycle slip corrections was 10.

For the analysis of the post-processed data, we used software programs in Fortran g95, C++, and Phyton programming languages, developed at the Institute of Geodesy and Geoinformatics (GGI).

The Bernese GNSS Software v5.2 post-processed data solutions were validated. The positioning results with discrepancies of > 10 cm were compared with filtrated average monthly station coordinates. The obtained solutions were considered faulty solutions if the values of discrepancies differed by more than the threshold of ±10 cm (Northing, Easting, Up, or summarized sqrt($dN^2 + dE^2 + dh^2$)). The analysis methodology using the software developed by the authors will be explained in presentation.

The analysis of space weather impacts on GPS positioning in Latvian CORS stations found strong degradation during the St Patricks' day geomagnetic storm on March 17, 2015. However, the less degraded results were fixed daily in post-midnight/predawn ionospheric scintillations for the entirety of March 2015. The sets of simultaneously occurring discrepancies over the network of CORS stations that were formed by a subset of CORS stations were named discrepancy clouds due to the electron density irregularity in the ionosphere, which can also be considered as the electron cloud, similar to molecular clouds in [8]. The cases of degraded results were searched in suspicion of a space weather impact on GPS observation results in the entire observation series in March 2015. In the frame of this study, the discrepancy clouds were analyzed. The discrepancies distribution and correlation analysis in discrepancy peaks, as well as the correlation with ROTI instead of TEC because the bins of ROTI information were much smaller than the max TEC values per day, were applied in Bernese GNSS Software v5.2 solutions. The whole set of disturbed solutions/stations with associated subsets of discrepancies and ROTI values for analysis was divided into three analyzed subsets.

The conclusion of the study was that each "shot" after 90 seconds gave a completely new cloud with a new impacted station subset, its configuration, and completely irregular discrepancy values. Following analysis of the positioning discrepancy clouds, the results revealed were as follows:

In plots of time series of sequentially disturbed solutions, the discrepancy size distribution was irregular and could not be predicted;

In the count of faulty solutions per station, the mean per month was 221 in 30 'calm' days and 319 per station in one day of the storm;

The mean discrepancy for 'calm' days was 0.92 m and for the day of the storm was 4.52 m;

The standard deviation of the discrepancy of 'calm' days was 3.39 m and was 12.75 m for the storm day;

Each "shot" after 90 seconds gave a completely new cloud, with a new impacted station subset, its configuration, and completely irregular discrepancy values;

The duration of Loss-of-Lock was long for Latvian CORS stations up to 4 hours for IRBE station (Fig. 1);

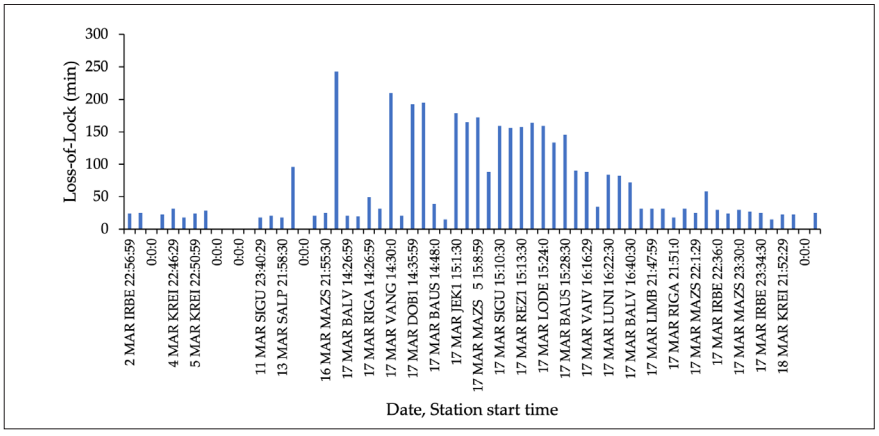

Fig. 1. Latvian CORS stations and their respective Loss-of-Lock start times and durations in minutes

The fluctuation of discrepancies during the geomagnetic storm in meters for Northing was [–130.5; 106.9], Easting [–74.9; 120.5], and Up [–531.6; 154.6];

The Pearson's correlation computed between discrepancies and ROTI values appeared weak;

The Pearson's correlation computed between discrepancies of monthly peak subsets was moderate;

The fluctuation of sites in discrepancy clouds was more intense on 'calm' days (Fig. 2). During the storm, the boundaries of adjacent clouds were more stable because all the CORS stations were impacted.

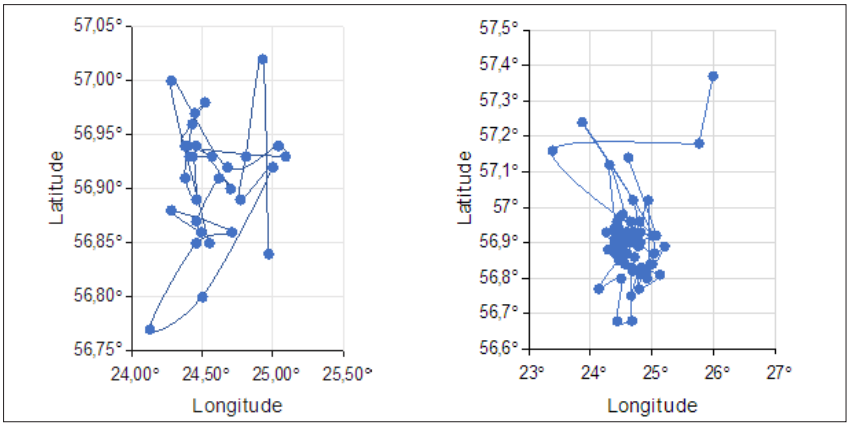

Fig. 2. Center coordinate variations for 36 peak clouds on the calm days in March 2015 (on the left side) and 149 clouds during the geomagnetic storm on March 17 (on the right side)

The area of analysis on March 16–18 was increased by including the EGNOS ground based Ranging and Integrity Monitoring Stations (RIMS): GVLA and GVLB, LAPA and LAPB, and WRSA and WRSB. The duration of Loss-of-Lock for EGNOS ground based RIMS stations lasted up to 10 hours in St. Patrick's Day geomagnetic storm.

The original article of the study is published in [9].

References

[1] Lu, Y.; Wang, Z.; Ji, S.; Chen, W. Assessing the Positioning Performance Under the Effects of Strong Ionospheric Anomalies with Multi-GNSS in Hong Kong. *Radio Sci.* **2020**, *55*, https://doi.org/10.1029/2019RS007004.

[2] Astafyeva, E.; Zakharenkova, I.; Förster, M. Ionospheric Response to the 2015 St. Patrick's Day Storm: A Global Multi-Instrumental Overview. Journal of Geophysical Research: Space Physics. **2015**, 120 (10): 9023–37. https://doi.org/10.1002/2015JA021629.

[3] Cherniak, I.; Zakharenkova, I.; Redmon, Robert J. Dynamics of the High-Latitude Ionospheric Irregularities during the 17 March 2015 St. Patrick's Day Storm: Ground-Based GPS Measurements. *Space Weather*. **2015**, 13 (9): 585–97. https://doi.org/10.1002/2015SW001237.

[4] Jacobsen Knut, Stanley; Yngvild Linnea, Andalsvik. Overview of the 2015 St. Patrick's Day Storm and Its Consequences for RTK and PPP Positioning in Norway. *Journal of Space Weather and Space Climate*. **2016**, 6 (February): A9. https://doi.org/10.1051/swsc/2016004.

[5] Liu, Jing; Wenbin, Wang, Alan Burns, Xinan Yue; Shunrong Zhang; Yongliang, Zhang; Chaosong, Huang. Profiles of Ionospheric Storm-enhanced Density during the 17 March 2015

Great Storm. *Journal of Geophysical Research: Space Physics.* **2016**, 121 (1): 727–44. https://doi.org/10.1002/2015JA021832.

[6] Yang, Z.; Morton, Y.T.J.; Zakharenkova, I.; Cherniak, I.; Song, S.; Li, W. Global View of Ionospheric Disturbance Impacts on Kinematic GPS Positioning Solutions During the 2015 St. Patrick's Day Storm. *J Geophys Res Space Phys.* **2020**, *125*, https://doi.org/10.1029/2019JA027681.

[7] Dach, R.; Lutz, S.; Walser, P.; Fridez, P. Bernese GNSS Software Version 5.2. **2015**, doi:10.7892/boris.72297.

[8] Baghmanyan, V.; Peron, G.; Casanova, S.; Aharonian, F.; Zanin, R. Evidence of Cosmic-Ray Excess from Local Giant Molecular Clouds. *Astrophys J.* **2020**, *901*, L4, https://doi.org/10.3847/2041-8213/abb5f8.

[9] Balodis, J.; Normand, M.; Zarins, A. The Movement of GPS Positioning Discrepancy Clouds at a Mid-Latitude Region in March 2015. Journal: Remote Sens. **2023**, Volume 15, Issue 8. Special Issue Applications of Remote Sensing in Monitoring Ionospheric Physics and Ionospheric Weather Forecasting. 20 pages and Supplementary files. https://doi.org/10.3390/rs15082032.

AFFECTION OF THE GPS SIGNAL L5 ON MULTIPATH ERROR MITIGATION IN DIFFERENTIAL POSITIONING SOLUTIONS

Mohamed Abdelhamid[1, 2], **Kamil Maciuk**[1]

[1] *Department of Integrated Geodesy and Cartography, AGH University, Krakow, Poland*
[2] *Department of Civil Engineering, Helwan University, Cairo, Egypt*
E-mail: mashraf@agh.edu.pl

Multipath is one of the error sources in GNSS measurements [1]. C/A code multipath error might be reduced by implementing a software method that uses wavelet transform as a basic data processing trend [2]. A new technique described to separate multipath and the receiver tracking error to study multipath affection on airborne receivers [3]. A necessary operation in the high-precision GNSS positioning is double-difference integer ambiguity resolution. The proportion of success of integer ambiguity fixing is called the success rate [4]. The combined model is a new technique that improves the ambiguity success rate when a few numbers of the satellites' precise observations are available [5]. The wide lane (WL) ambiguity fixing rate was enhanced when using triple frequencies (L1 + L2 + L5) for approximately 100 km baseline length [6].

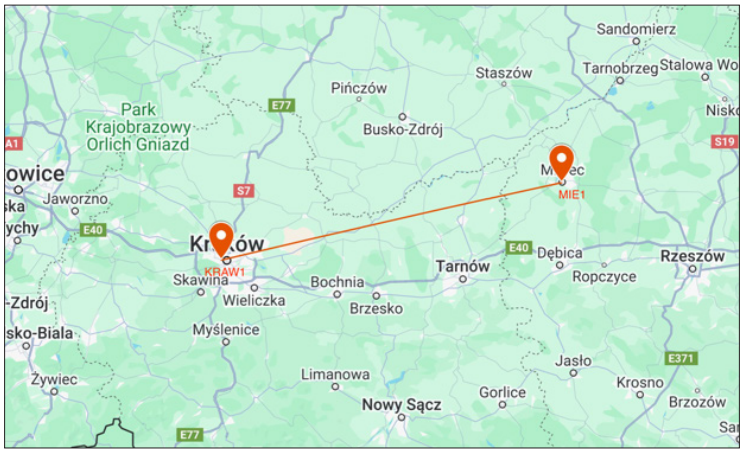

Fig. 1. Baseline map (maps.google.com)

This article discusses the effect of multipath error percentage on ambiguity fixing rate with dual GPS frequencies (L1 + L2) and triple GPS frequencies (L1 + L2 + L5). For that reason, simulated data for stations mentioned in Table and its plan illustrated in Fig. 1 has been used to study the ability to fix the ambiguity in different multipath proportions in the raw data. The selected positions are placed in Poland away from each other by approximately 110 km which is considered a long baseline. Data simulated with dual and triple frequencies at an observation rate of 0.10 HZ and cut of angle 10 degrees for two hours. The linear combinations that come from wide-lane (L1 + L2) and narrow-lane (L1 + L2) are used to fix the ambiguities [7].

Table. UTM Coordinates (Zone 34 U) of selected Stations in Poland for creating the simulated data

Station	E (m)	N (m)	h (m)
KRAW1	422706.370	5546527.540	267.110
MIE1	529921.810	5570403.450	227.596

The triple-frequency linear combination is used which has been described below equation [8].

$$\nabla\Delta\phi_{LC} = \left(\frac{K1}{\lambda_1} + \frac{K2}{\lambda_2} + \frac{K3}{\lambda_3}\right)(\nabla\Delta R + \nabla\Delta dR + \nabla\Delta T) - \left(K_1\frac{1}{\lambda_1} + K_2\frac{\lambda_2}{\lambda_1^{\,2}} + K_3\frac{\lambda_3}{\lambda_1^{\,2}}\right)\nabla\Delta I_1 - \nabla\Delta N_i + \left(\frac{K_1}{\lambda_1} + \frac{K_2}{\lambda_2} + \frac{K_3}{\lambda_3}\right)\nabla\Delta\varepsilon_{\emptyset_i}$$

Where $\nabla\Delta\phi_{LC}$ is the DD phase linear combination (cycles); K_1, K_2, and K_3 are the oefficients. λ_1 is the wavelength of the i-th carrier frequency (i = 1, 2, 3); $\nabla\Delta$ is the DD operator $\emptyset_i$ is the phase observation on the i-th carrier frequency, in cycles (i = 1, 2, 3); R is the geometric range (meter); dR is the orbital error (meter); I_1 is the ionospheric delay (meter) on the 1st carrier frequency $L1$; T is the tropospheric delay (meter); N_i is the phase ambiguity (cycles) of the i-th carrier frequency and $\varepsilon_{\emptyset_i}$ is the phase noise (including receiver noise and multipath). The authors changed every time in the simulated data the percentage of multipath from 10 % to 80 % from the raw data, the results showed that by using dual frequencies, there is no solution but it's easy to fix the ambiguities with the triple frequencies.

Fig. 2 shows that the percentage of success rate decreases with increasing the multipath ratio in raw data, but the solution could be achieved using triple frequencies. Raw data with 10 % multipath led to approximately 62 % success rate, 40 % multipath led to approximately 10 % success rate, and from 50 % until the end, the success rate fluctuated around 9 %.

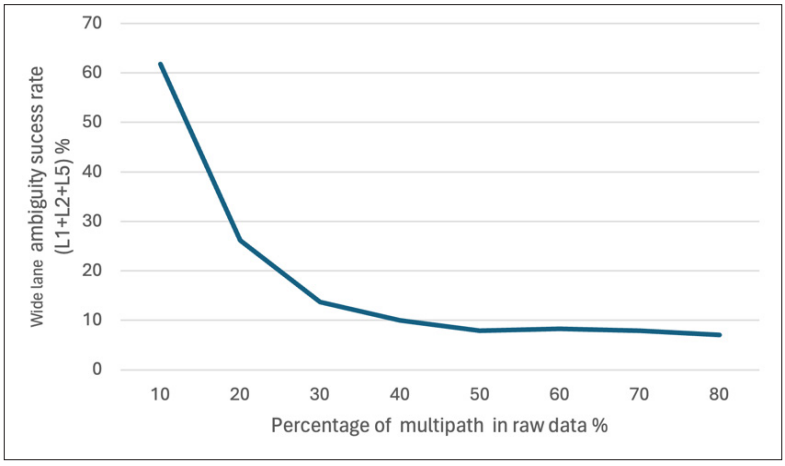

Fig. 2. Ambiguity success rate using triple frequencies in different multipath percentages in raw data

Analyses in this paper deal with the impact of multipath error on the number of ambiguity success rates using triple frequencies. Results show a high correlation between the number of observations affected by a multipath error with a wide lane ambiguity success rate.

References

[1] Estimation of Multipath Error in GPS Pseudorange Measurements. Navigation, 44(1), 43–52 | 10.1002:j.2161-4296.1997.tb01938.x.

[2] Azarbad M. R.; Mosavi M. R. A new method to mitigate multipath error in single frequency GPS receiver with wavelet transform. *GPS Solutions*. Apr. **2014**, vol. 18, no. 2, 189–198, https://doi.org/10.1007/s10291-013-0320-1.

[3] Isolation of GPS Multipath and Receiver Tracking Errors. Navigation, 41(4), 415–435 | 10.1002:j.2161-4296.1994.tb01888.x.

[4] Amiri-Simkooei, A. R.; Jazaeri, S.; Zangeneh-Nejad, F.; Asgari, J. Role of stochastic model on GPS integer ambiguity resolution success rate. *GPS Solutions*. Jan. **2016**, vol. 20, no. 1, 51–61, https://doi.org/ 10.1007/s10291-015-0445-5.

[5] Wu, S.; Zhao, X.; Pang, C.; Zhang, L.; Xu, Z.; Zou, K. Improving ambiguity resolution success rate in the joint solution of GNSS-based attitude determination and relative positioning with multivariate constraints. *GPS Solutions*. Jan. **2020**, vol. 24, no. 1, https://doi.org/10.1007/s10291-019-0943-y.

[6] Ali, E.-S. IMPACT OF USING THE NEW THIRD FREQUENCY ON GPS AMBIGUITY RESOLUTION. **2020**.

[7] Teunissen, P. J. G.; Tiberius, C. C. J. M.; Joosten, P. Geometry-free Ambiguity Success Rates in Case of Partial Fixing. **1999**. [Online]. Available: https://www.researchgate.net/publication/266016106.

[8] Zhang, W. UNIVERSITY OF CALGARY Triple Frequency Cascading Ambiguity Resolution for Modernized GPS and GALILEO. **2005**.

GNSS LEVELLING – AN OPTIMISED GNSS SESSION FOR 1ST CLASS LEVELLING NETWORK

Łukasz Borowski[1], Piotr Banasik[2], Kamil Maciuk[2]

[1] *Department of Ecological Engineering and Forest Hydrology, Faculty of Forestry, University of Agriculture in Krakow, Mickiewicz av. 24, Krakow, Poland, ORCID: 0000-0001-7356-5377*
[2] *Department of Integrated Geodesy and Cartography, AGH University of Krakow, Mickiewicz av. 30, Krakow, Poland, ORCID: 0000-0002-3604-4019, 0000-0001-5514-8510*
E-mail: lukasz.borowski@urk.edu.pl

The Polish state 1st class levelling network has over 40,000 points. Its partial modernization took place in 1999–2012 [1] [2], as a result of which the PL-EVRF2007-NH vertical frame was introduced. The 20-year period between the modernization of the network (the so-called Measuring Campaigns) indicates the need to perform such in the coming years. In 2016 the Head Office of Geodesy and Cartography (HOGC) reported that in 20 years the network had about 23 % points getting lost [3]. Therefore, the new levelling network will be limited to main lines with about 16,000 points. It will maintain a height connection between the most important network points, like the satellite stations ASG–EUPOS, with neighbouring countries [4]. Current regulations require an accuracy of 1.5 mm/km, less than the last one (1 mm/km), this follows the trend away from the highest possible accuracy [4] [5], whether declarative or real one. So far, the levelling lines were routed to cross each of the 380 powiats (second level of Polish administrative division). The reduced network will remain powiats without 1st class points (or with a limited number). Gap filling will be provided by GNSS levelling, which is a cost-effective method and additionally makes possible to bypass terrain obstacles [6] (e.g. rivers). All the points, whether established in by precise geometric or GNSS levelling, will be adjusted in one-step process and require the same accuracy level (1.5 mm/km).

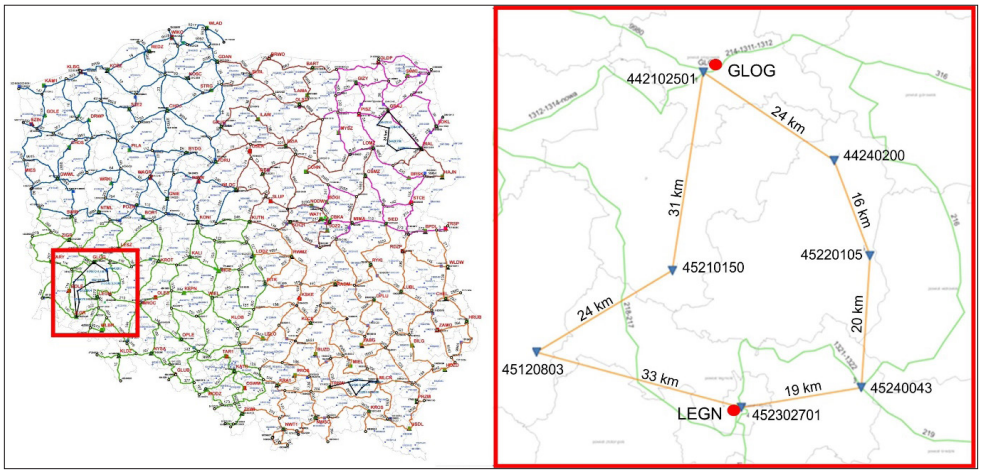

Fig. 1. The experiment localisation on the levelling network (left) and close up to points and vectors (right), with two ASG-EUPOS stations. Own study based on HOGC tender documentation.

Because satellite levelling has never been used to date for such works, no regulations were implemented. The ones in use date from 2002 [7], i.e. before permanent GNSS station systems were widespread. For this reason, the Head Office of Geodesy and Cartography commissioned a measurement experiment, which will be used to develop new regulations for the vertical network modernisation process.

The presentation shows the results of the experiment. The measurement (Fig. 1) was carried out for 7 points of the existing 1st class matrix, of which 2 are excentres of the ASG-EUPOS network. Unlike other studies, the aim was not to achieve the highest GNSS levelling accuracy (e.g. [8]) but to determine the accuracy achieved by an 'average' surveying company. Therefore, neither antennas with individual calibration, nor the Bernese GPS Software was used. Typical geodetic equipment in the form of SatLab Freya integrated antenna receivers was used and vectors were calculated in the Trimble Business Center 5 software. Observations were performed for two days synchronously over 12 hours each with A 5° elevation mask. As a result, the height differences between the points were calculated, which were converted to normal altitudes through the national quasi-geoid model PL-geoid2021 [9] (system PL-ETRF2000, PL-EVRF2007-NH) according to the formula:

$$\Delta H_{AB}^{n} = \Delta h_{AB}^{e} - \Delta \zeta_{AB} \tag{1}$$

ΔH_{AB}^{n} – normal height difference between point A and B,

Δh_{AB}^{e} – ellipsoid height difference,

$\Delta \zeta_{AB}$ – normal undulation difference taken form quasi-geoid model.

The analysis of the results was carried out for 2,4,6,8 and 12-hour sessions, in the adopted GNSS systems: (1) GPS only, (2) GPS+Galileo, (3) GPS+Galileo+GLONASS, and (4) GPS+Galileo+GLONASS+Beidu. For each session, two vector solutions were performed (a) inimal – the vectors connect the points as they would be measured by geometric levelling, and (b) each point with each (8 vectors were calculated for each point: 6 for the points and two for the nearest ASG–EUPOS stations). A total of 40 calculation scenarios were analysed. In each case, the height difference results from the vector calculation, not the coordinate difference. The exception was a single scenario (41th) based on the absolute PPP (Precise Point Positioning) method calculated for a 12-hour session of GPS+Galileo+GLONASS+Beidu systems by the Canadian Geodetic Survey server for automatic calculation called CSRS-PPP [8].

References

[1] Borowski, Ł.; Kubicki, B.; Gołąb, J. Implementation of the EVRF2007 Height Reference Frame in Poland. *Journal of Applied Geodesy.* **2023**, 17 (4), 313–323. https://doi.org/10.1515/jag-2023-0020.

[2] Borowski, L.; Banasik, P. The Conversion of Heights of the Benchmarks of the Detailed Vertical Reference Network into the PL-EVRF2007-NH Frame. *Reports on Geodesy and Geoinformatics.* **2020**, 109 (1), 1–7. https://doi.org/10.2478/rgg-2020-0001.

[3] Graszka, W.; Pielasa, E.; Wajda, S.; Piętka, D. Podstawowa Osnowa Wysokościowa, Grawimetryczna i Magnetyczna – Ocena Stanu i Prognozy Rozwoju. In *Współczesne problemy podstawowych osnów geodezyjnych w Polsce*; Komitet Geodezji PAN: Grybów, **2016**.

[4] Cvetkov, Vasil. Two adjustments of the second levelling of Finland by using nonconventional weights. *Journal of Geodetic Science.* **2023**, 13 (1), 20220148. https://doi.org/10.1515/jogs-2022-0148.

[5] Apollo, M.; Jakubiak, M.; Nistor, S.; Lewinska, P.; Krawczyk, A.; Borowski, Ł.; Specht, M.; Krzykowska-Piotrowska, K.; Marchel, Ł.; Pęska-Siwik, A.; Kardoš, M.; Maciuk, K. Geodata in Science – a Review ff Selected Scientific Fields. ASP.FC. **2023**, 22 (2), 17–40. https://doi.org/10.15576/ASP.FC/2023.22.2.02.

[6] Banasik, P.; Bujakowski, K. The Use of Quasigeoid in Leveling Through Terrain Obstacles. *Reports on Geodesy and Geoinformatics.* **2018**, 104 (1), 57–64. https://doi.org/10.1515/rgg-2017-0015.

[7] Kmiecik, J.; Zygierewicz, Z.; Ryszard, O. Wytyczne Techniczne G-1.11 Podstawowa Osnowa Wysokościowa. Projektowanie, Pomiar i Opracowanie Wyników; Głowny Geodeta Kraju: Warszawa, **2002**.

[8] Stepniak, K.; Baryła, R.; Wielgosz, P.; Kurpinski G. Optimal Data Processing Strategy in Precise GPS Leveling Networks. Acta Geodyn. Geomater. **2013**, 10 (4), 443–452. https://doi.org/10.13168/AGG.2013.0044.

[9] Canadian Geodetic Survey. *Precise Point Positioning* (CSRS-PPP). **2023**. https://webapp.csrs scrs.nrcan-rncan.gc.ca/geod/tools-outils/ppp.php.

SATELLITE-BASED EVAPOTRANSPIRATION ESTIMATION: A COMPREHENSIVE REVIEW

Lachezar Filchev

Space Research and Technology Institute, Bulgarian Academy of Sciences (SRTI-BAS), Acad. G. Bonchev str.1, Sofia, Bulgaria
E-mail: lachezarhf@space.bas.bg

Satellite-based estimation of evapotranspiration (ET) has emerged as a vital tool in hydrological and agricultural studies due to its wide spatial coverage and temporal resolution [1–4]. This paper presents a comprehensive review of existing methodologies, datasets, and challenges associated with satellite-derived ET estimation [5–8]. We systematically evaluate the strengths and limitations of various satellite sensors and retrieval algorithms utilized in estimating ET over different spatial and temporal scales [9–11]. Additionally, we discuss the uncertainties inherent in satellite-based ET products and explore strategies for improving their accuracy and reliability [12–15]. Furthermore, we highlight the applications of satellite-based ET estimation in water resource management, agricultural productivity assessment, and climate change studies [16–20]. By synthesizing current knowledge and identifying future research directions, this review aims to provide a valuable resource for researchers, practitioners, and policymakers involved in the utilization of satellite data for understanding the complex dynamics of evapotranspiration processes at regional to global scales [21–28].

References

[1] Evaluation of Spatio-Temporal Evapotranspiration Using Satellite-Based .... https://link.springer.com/article/10.1007/s12524-021-01367-w.

[2] Satellite-based estimation of actual evapotranspiration in the Buyuk .... https://iwaponline.com/hr/article/48/2/559/1962/Satellite-based-estimation-of-actual.

[3] An Experimental Study on Evapotranspiration Data Assimilation Based on .... https://link.springer.com/article/10.1007/s11269-016-1485-5.

[4] Evapotranspiration estimation using a satellite-based surface energy .... https://link.springer.com/article/10.1007/s12665-023-11284-5.

[5] Satellite Remote Sensing for Estimating PM2.5 and Its ... – Springer. https://link.springer.com/article/10.1007/s40726-020-00170-4.

[6] Use and Impact of Satellite-Derived SST Data in a Global Ocean .... https://link.springer.com/article/10.1007/s12524-022-01586-9.

[7] A Review on Estimation of Particulate Matter from Satellite-Based .... https://link.springer.com/article/10.1007/s13143-020-00215-0.

[8] Review on spatial downscaling of satellite derived precipitation .... https://link.springer.com/article/10.1007/s12665-023-11115-7.

[9] Remote Sensing Precipitation: Sensors, Retrievals, Validations, and .... https://link.springer.com/referenceworkentry/10.1007/978-3-662-47871-4_4-1.

[10] Frontiers | Grand Challenges in Satellite Remote Sensing. https://www.frontiersin.org/articles/10.3389/frsen.2021.619818/full.

[11] Advances in Precipitation Retrieval and Applications from Low-Earth .... https://journals.ametsoc.org/downloadpdf/view/journals/bams/104/10/BAMS-D-23-0229.1.pdf.

[12] Discovering Optimal Triplets for Assessing the Uncertainties of ... – MDPI. https://www.mdpi.com/2072-4292/15/13/3215.
[13] Uncertainty Assessment of Satellite Remote Sensing – based .... https://egusphere.copernicus.org/preprints/2023/egusphere-2023-725/egusphere-2023-725.pdf.
[14] Quantifying the Reliability and Uncertainty of Satellite, Reanalysis .... https://www.mdpi.com/2072-4292/15/1/213.
[15] A global map of uncertainties in satellite-based precipitation measurements. https://agupubs.onlinelibrary.wiley.com/doi/pdf/10.1029/2010GL046008.
[16] Water | Free Full-Text | Estimation of ET and Crop Water Productivity .... https://www.mdpi.com/2073-4441/16/3/422.
[17] Evapotranspiration estimation using Surface Energy Balance ... – Nature. https://www.nature.com/articles/s41598-023-38563-2.pdf.
[18] Application of Satellite Remote Sensing to Regional Agriculture and .... https://www.un-spider.org/sites/default/files/session2-5-masahirotasumi-application-of-satellite-remote-sensing-to-regional-agriculture-and-water-resource-management.pdf.
[19] ARSET – Applications of Remote Sensing-Based Evapotranspiration ... – NASA. https://appliedsciences.nasa.gov/get-involved/training/english/arset-applications-remote-sensing-based-evapotranspiration-data.
[20] A new, rigorous assessment of OpenET accuracy for supporting satellite .... https://www.sciencedaily.com/releases/2024/01/240116191503.htm.
[21] Toward More Integrated Utilizations of Geostationary Satellite Data for .... https://www.mdpi.com/2072-4292/13/8/1553.
[22] Satellite Altimetry for Ocean and Coastal Applications: a Review – MDPI. https://www.mdpi.com/2072-4292/15/16/3939.
[23] Research development, current hotspots, and future directions of water .... https://link.springer.com/article/10.1007/s11356-017-9107-1.
[24] On the Use of Interferometric Synthetic Aperture Radar Data for .... https://link.springer.com/article/10.1007/s11004-021-09948-8.
[25] An Overview of the Applications of Earth Observation Satellite Data .... https://www.mdpi.com/2072-4292/14/8/1863.
[26] Sea Ice Extraction via Remote Sensing Imagery: Algorithms, Datasets .... https://www.mdpi.com/2072-4292/16/5/842.
[27] Satellite Sensors and Retrieval Algorithms of Atmospheric Methane. https://www.researching.cn/articles/OJfb70b62a20c37744.
[28] Estimation of Satellite-Based Regional-Scale Evapotranspiration for .... https://link.springer.com/chapter/10.1007/978-3-031-12112-8_29.

ENHANCING EFFICIENCY THROUGH GEOINFORMATICS-DRIVEN TERRITORIAL REORGANIZATION

Peteris Daugulis

Institute of Life Sciences and Technologies, Daugavpils University,
Parades 1a, Daugavpils, Latvia
E-mail: peteris.daugulis@gmail.com

Efficient and equitable access to municipal services hinges on well-designed administrative divisions. It requires ongoing adaptation to changing infrastructure factors. We propose a novel transparent data-driven method for territorial division based on geospatial data, the Voronoi partition of edge-weighted road graphs and a special case of the minimax facility location problem [1]. By considering road network structure and strategic placement of administrative centers, this method seeks to minimize travel time disparities and ensure a more balanced distribution of administrative time burden for the population. We show implementations of this approach in the context of Latvia (see Fig. as an example).

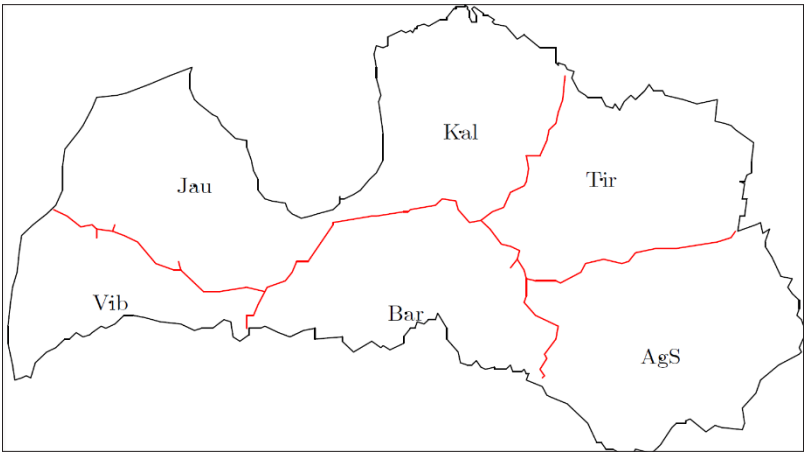

Fig. A division of Latvia into 6 territorial units satisfying the travel-time minimax principle

References

Daugulis, P. Optimizing Administrative Divisions: a Vertex k-Center Approach for Edge-Weighted Road Graphs. submitted.

SMART4COV19: AN INNOVATIVE APPROACH TO COVID–19 DETECTION AND MANAGEMENT USING SMART TECHNOLOGIES AND REMOTE SENSING

Lachezar Filchev, Maria Dimitrova, Georgi Jelev, Plamen Trenchev, Milen Chanev

Space Research and Technology Institute, Bulgarian Academy of Sciences (SRTI-BAS), Acad. G. Bonchev str.1, Sofia, Bulgaria
E-mail: lachezarhf@space.bas.bg

The COVID–19 pandemic has necessitated the rapid development and deployment of innovative solutions for detection, management, and mitigation [1–2]. "Smart4COV19: An Innovative Approach to COVID–19 Detection and Management Using Smart Technologies" presents a comprehensive overview of the Smart4COV19 project, which leverages smart technologies, including Artificial Intelligence (AI) and Internet of Things (IoT), and remote sensing to combat the COVID–19 pandemic [3]. The project focuses on the utilization of these technologies for early detection of the virus, efficient patient management, and effective resource allocation [4–5]. The paper discusses the integration of AI algorithms with IoT devices for real-time data collection, processing, and transmission, which has significantly improved the efficiency of COVID–19 detection and management [6, 7]. However, the implementation of these technologies also presents challenges, such as data privacy and security, interoperability, and the need for robust validation [8, 9]. The paper explores these challenges and proposes potential solutions, paving the way for the wider adoption of smart technologies in pandemic response [6, 10]. Finally, the paper outlines future research directions, emphasizing the need for continuous innovation and improvement in smart technologies for pandemic management [11, 7].

References

[1] Khan, H.; Kushwah, K. K.; Singh, S.; Urkude, H.; Maurya, M. R.; Sadasivuni, K. K. 3 Biotech. **2021**, 11 (2), 50.

[2] Whitelaw, S.; Mamas, M. A.; Topol, E.; Van Spall, H. G. C. Lancet Digit. Health. **2020**, 2 (8), e384-e395.

[3] World Economic Forum. 3 ways tech solutions can help the world tackle COVID–19. Available at: https://www.weforum.org/agenda/2020/11/3-ways-new-technology-solutions-can-help-the-world-fight-covid-19/.

[4] Hosseinifard, M.; Naghdi, T.; Morales-Narváez, E.; Golmohammadi, H. Front. Bioeng. Biotechnol. **2021**, 9, 637203.

[5] Routledge. Pandemic Detection and Analysis Through Smart Computing Technologies. Available at: https://www.routledge.com/Pandemic-Detection-and-Analysis-through-Smart-Computing Technologies/Raw-Jain-Das-Sharma/p/book/9781774910320.

[6] IEEE. Artificial Intelligence, Machine Learning & Internet of Medical Things for COVID–19. Available at: https://smartcities.ieee.org/newsletter/august-2021/artificial-intelligence-machine-learning-internet-of-medical-things-iomt-for-covid-19-future-pandemics-an-exploratory-study.

[7] Frontiers. Applying robotics and AI in pandemics (COVID–19): Detection, diagnosis, and delivery. Available at: https://www.frontiersin.org/articles/10.3389/frobt.2022.1039273/full.

[8] Ingenta Connect. COVID–19: Challenges and its Technological Solutions using IoT. Available at: https://www.ingentaconnect.com/content/ben/cmir/2022/00000018/00000002/art00004.

[9] Filchev, L.; Dimitrova, M.; Jelev, G.; Gochev, D.; Trenchev, P. Air quality CAMS data and products in Smart4COV19/Telemedicine project. Available at: https://atmosphere.copernicus.eu/sites/default/files/2022-12/19%20-%20Filchev%20-%20Air%20quality%20CAMS%20data%20and%20products%20in%20Smart4COV19Telemedicine%20project.pdf.

[10] Wang, L.; Zhang, Y.; Wang, D.; Tong, X.; Liu, T.; Zhang, S.; Huang, J.; Zhang, L.; Chen, L.; Fan, H.; Clarke, M. Front. Med. **2021**, 8, 704256.

[11] Abdulkareem, M.; Petersen, S. E.; Topol, E.; Van Spall, H. G. C. Front. Artif. Intell. **2021**, 4, 652669.

STUDYING SEASONALITY IMPACT ON TANDEM-X BISTATIC INSAR DATA OF FOREST ECOSYSTEMS IN BULGARIA

Zlatomir Dimitrov

Space Research and Technology Institute, Bulgarian Academy of Sciences,
Acad. Georgy Bonchev str., block 1, 1113 Sofia, Bulgaria
E-mail: zlatomir.dimitrov@space.bas.bg

Forest ecosystems are with high ecological and economical value, were forest biomass is major biophysical parameter in the global CO2 cycle, targeted at the REDD+ activities. Remote sensing for earth observation is widely utilized by means of optical and most recently SAR based methods to study forest perameters, where to derive above ground biomass (AGB) and forest height, as well as to study forest structure. SAR signal penetrates differently into the forest canopy in respect to the wavelength. This implies different sensitivity of the SAR method to the forest canopy structural parameters.

The SAR Interferometry (InSAR) is mostly sensitive to the vertical distribution of the phase scattering centers within the forest volume. The X-band DLR's bistatic InSAR TanDEM-X mission that is dedicated for generation of the high fidelity global digital elevation model, is well utilized in the forest studies to derive canopy height model. It is found that the bistatic InSAR coherence is a general parameter that is sensitive to the forest structure and could derive forest structural parameters. Volumetric decorrelation is highly observed in forest ecosystems and its loss depends on the biomass levels. Seasonality changes are causing coherence loss in spring in the non-frozen period of the year, or increasing coherence during the winter in the sake of frozen conditions. It is shown that coniferous species exhibits lower coherence loss rather than deciduous species during frozen conditions. During seasonal change in spring and autumn, the variation between frozen and unfrozen conditions is very common, especially in mountainous temperate forests in Bulgaria at higher altitudes above sea level, which could cause ice and snow breakage hitting large scale of the forest territory.

The seasonality changes that impact the SAR signal are not well studied in Bulgarian forest ecosystems via SAR methods. This study focusses on amplitude and phase analyis based on bistatic InSAR measurements from TanDEM-X, in two types of forest ecosystems. First biome is flat dingy forest with high forest density and height, near black sea coast of Bulgaria, comprising the biosphere reserve (BR) of „Kamchia". The second biome is mountainous temperate mixed forest in the north-west of the Balkan mountain massif in rugged terrain. Four single polarization and two dual polarization bistatic TanDEM-X measurements in stripmap mode were utilized in this study.

In the amplitude analysis, RGB combination were elaborated from the InSAR coherence, phase and intensity for better representation of the InSAR observables from TanDEM-X, to represent physical differences of natural targets. Winter measurements showed high penetration in X-band into the canopy revealing backscatter from the forest's understorey. Due to higher resolution of the products local roads and forest paths are prominent in the summer

acquisitions. In the mountains geometric distortions are general issue in the TanDEM-X imagery.

In the flat dingy forest, phase analysis showed that coherence is rather higher during leaf-off in late autumn due to wet conditions and higher penetration, resulting better sensitivitiy to the forest volume. Intensity is 2 dB lower in summer conditions rather than winter, due to higher energy loss from the canopy during leaf-on. Coherence loss in areas with small incidence angles found to be higher in winter. Elaborated transect in decidous forest showed high penetration during winter and leaf-off, with differences more than 10 meters between scattering phase centers vertical location in both seasons. Conducted phase analysis on different species for winter and summer showed highest differences amongst deciduous forest speices rather coniferous ones. Statistical analysis also confirmed highest differences for deciduous species.

Dual polarization TanDEM-X products showed certain differences early and late spring after leaf-on, suggesting more dihedtral scattering contribution during leaf-off.

The TanDEM-X InSAR bistatic data showed high contrast of the scattering phase centers vertical location in depend of seasonality. The TanDEM-X bistatic InSAR data is well utilized to represent differences in the sake of environemntal factors in the forest ecosystems.

COMPARISON OF TWO DEEP LEARNING MODELS TO DETERMINE BURNED FOREST AREAS FROM SENTINEL-2 IMAGERY

Ahmet Kılıç[1], Bahadır Kulavuz[2], Tolga Bakirman[2], Bulent Bayram[2]

[1] *Yildiz Technical University, Graduate School of Science and Engineering, Division of Data Science and Big Data, 34220 Esenler, Istanbul, Türkiye*
[2] *Yildiz Technical University, Civil Engineering Faculty, 34220 Esenler Istanbul, Türkiye*
E-mail: bahadir.kulavuz@yildiz.edu.tr

Forests are complex ecosystems that host more than 70 % of the Earth's biodiversity. Forests, which are also of critical importance for the sustainability of life, help reduce the greenhouse gas effect by absorbing carbon dioxide in the atmosphere and play an important role in balancing atmospheric conditions. It also contributes to protecting water resources, preventing soil erosion and reducing air pollution. Protecting and sustainably managing forests, which are the centre of natural life and indispensable for the sustainability of life, has vital importance for nature and human beings. Forest fires, which play a major role in the destruction of forests, are devastating events that occur due to natural or human-induced causes and threaten the ecological balance. In this study, it is suggested to use deep learning techniques to segment burned forest areas to effectively analyse forest losses caused by forest fires and to correctly implement improvement works.

The open-access Satellite Burned Area Dataset is used to create burned area segments from Sentinel-2 images. Although this dataset has been prepared for burn severity mapping with 6 classes (the first 5 classes represent the burn severity and the 6th class represents background). In this study, only 73 labelled images have been used and 690 image patches have been created in 256 × 256 pixel size. 552 and 138 image patches have been used for training and testing of both models. These sub-datasets have been generated for R, G, B and R, G, NIR Sentinel-2 bands for two classes which are background and burned areas. The first class represents unburned areas which are generated by merging of background and two burned area classes from the original dataset. The burned area class is generated by merging three burned area classes (moderate severity, high severity and extreme severity) from the original dataset. The image patches which consist of more than 98 % background have been eliminated to obtain our sub-dataset.

UNet and FPN architectures have been used for binary burned area semantic segmentation. The same hyperparameters for both architectures have been used. resnet18 encoder, imagenet's weights have been used for model training. The used loss function is the sum of the dice loss and focal loss functions. The obtained IoU scores for RGB dataset are 45.7 % for UNet and 42.3 % for FPN respectively. The IoU scores for RGNIR dataset are 76 % for UNet and 75.2 % for FPN respectively.

The results show that there are no significant differences between the two models.